Fluid Dynamics on Logarithmic Lattices and Singularities of Euler Flow

Master's Thesis

by
Ciro Sobrinho Campolina Martins

Advisor: Alexei A. Mailybaev

Instituto de Matemática Pura e Aplicada

Rio de Janeiro, February 2019

A thesis submitted in fulfilment of the requirements for the degree of Master of Science at the Insituto de Matemática Pura e Aplicada – IMPA.

Approved on February 26, 2019, by the committee:

Alexei Mailybaev (advisor) – IMPA

André Nachbin – IMPA

Simon Thalabard – IMPA

Dan Marchesin – IMPA

To my grandparents Hilton (*in memoriam*)
and Selma Sobrinho, with love.

Acknowledgements

I would like to express my gratitude to my advisor, Alexei Mailybaev, for sharing his ideas and his enthusiasm during our research. I would like to thank also:

Professors André Nachbin, Simon Thalabard and Dan Marchesin, for their useful comments and suggestions on this thesis.

The Fluid Dynamics group of IMPA, for the stimulating research environment and for welcoming me as part of the family; in particular, Guilherme Tegoni, for his support and friendship during my first steps at IMPA.

My mother and father, Claudia and Antonio Henrique, and my brothers and sister, Joana, André and Antônio, for their constant encouragement througout this period.

My grandmother, Selma, for giving me a lovely home at Rio.

Finally, I would like to thank CNPq, for the financial support.

Now we have already not a single mathematical space, but infinitely many of them, and it is unknown which one is the most adequate model of the space of the physical reality.

Modern controversies on the nature of Mathematics
A. N. Kolmogorov

Abstract

The dispute on whether the three-dimensional (3D) incompressible Euler equations develop an infinitely large vorticity in a finite time (blowup) keeps increasing due to ambiguous results from state-of-the-art direct numerical simulations (DNS), while the available simplified models fail to explain the intrinsic complexity and variety of observed structures. Here, we propose a new technique, which considers the Fluid Dynamics equations restricted to a logarithmic lattice in Fourier space with specially designed calculus and algebraic operations, giving rise to simplified models structurally identical to the original ones. The application of this technique to the 3D Euler flow clarifies the present controversy at the scales of existing DNS and provides unambiguous evidence of the following transition to the blowup, explained as a chaotic attractor in a renormalized system. The chaotic attractor has an anomalous multiscale structure, suggesting that the existing DNS strategies at the resolution accessible now (and presumably rather long into the future) may be unsuitable for the analysis of blowup.

Table of contents

Chapter 1

Introduction

Turbulence remains one of the most important unsolved problems in Classical Physics. A number of natural phenomena, ranging from ocean and atmosphere dynamics to the formation of galaxies, is related to turbulence and defies a satisfactory theoretical explanation. Furthermore, the extent of its applications in industry reinforces the need for a reliable physical description: the increase of mixing rate in combustion engines and chemical reactors, the reduction of drag in aircraft design, and weather forecasting are just a few examples of turbulence-related thecnological problems with great impact on our daily experience.

One of the greatest challenges in turbulence lies on how to recover its phenomenological theory from first dynamical principles, or, in other words, from the governing equations of Fluid Dynamics. It is widely accepted that simple fluids are described by the incompressible Navier-Stokes equations, which in dimensionless form read

$$\partial_t \mathbf{u} + \mathbf{u} \cdot \nabla \mathbf{u} = -\nabla p + \frac{1}{Re} \Delta \mathbf{u}, \quad \nabla \cdot \mathbf{u} = 0, \tag{1.1}$$

where $\mathbf{u} = (u_1, u_2, u_3)$ is the velocity field and p is the scalar pressure; Re is the Reynolds number defined as $Re = UL/\nu$, where U and L are characteristic velocity and length of the flow, respectively, and $\nu \geq 0$ is the kinematic viscosity. The divergence free condition $\nabla \cdot \mathbf{u} = 0$ is the mathematical constraint of incompressibility. The viscous force $\frac{1}{Re}\Delta \mathbf{u}$ has the form of a diffusion term and acts in the system as a smoother of irregularities. For high viscosity, the diffusion term is dominant and the flow is smooth and regular, while as the viscosity decreases, the nonlinearities prevail and the fluid motion becomes more chaotic and unpredictable. In this setting, ideal turbulence is usually associated with the assymptotic limit $\nu \to 0$, or equivalently $Re \to \infty$.

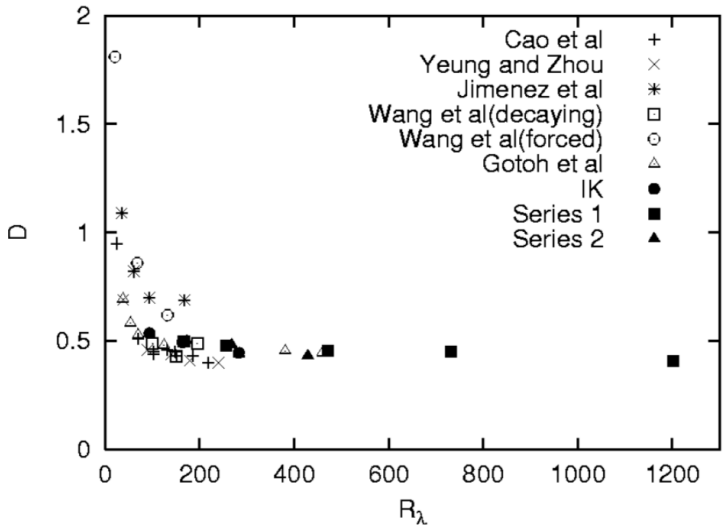

Fig. 1.1 Normalized energy dissipation rate $D = \langle\varepsilon\rangle L/U^3$ versus Taylor microscale Reynolds number R_λ from numerical experiments. The energy dissipation attains a nonzero value in the limit $R_\lambda \to \infty$. Figure taken from [49].

When the viscosity is set to zero, $\nu = 0$, the equations (1.1) become

$$\partial_t \mathbf{u} + \mathbf{u} \cdot \nabla \mathbf{u} = -\nabla p, \quad \nabla \cdot \mathbf{u} = 0, \tag{1.2}$$

and are referred to as the Euler equations for incompressible ideal flow, since the viscous dissipative term is dropped. In fact, it is not difficult to show that smooth solutions $\mathbf{u}$ of this system conserve the energy $E = \frac{1}{2}\int |\mathbf{u}|^2 d\mathbf{x}$ in time.

By regarding equations (1.2) as the limit case $\nu \to 0$ of the Navier-Stokes system, the Euler equations are expected to describe the dynamics of turbulent flows. However, an experimental fact apparently defies this intuitive idea: the energy dissipation $\varepsilon = \nu|\nabla \mathbf{u}|^2$ seems not to vanish in the limit $\nu \to 0$ [49, 68], a phenomenon known as *anomalous dissipation* — see Fig. 1.1. This might look paradoxical at first sight, since the Euler equations consitute a conservative system. Nevertheless, Onsager [67, 34] was the first to notice that the Euler equations need not to conserve energy if they are not sufficiently regular. He conjectured that non-vanishing energy dissipation in high-Reynolds-number turbulence is associated to singular (distributional) solutions of the incompressible Euler equations, a statement under active research nowadays [33, 20, 14, 48, 13].

Thus, Onsager linked the physical feature of anomalous dissipation in turbulent flows to the mathematical regularity of Euler solutions. Accordingly, aiming a deep understanding of turbulence, one may formulate the following fundamental question:

how regular are the solutions of the Euler equations?

To discuss the regularity of Euler solutions, it is usefull to introduce the vorticity field $\boldsymbol{\omega} = \nabla \times \mathbf{u}$. If we take the curl of equations (1.2), one obtains, after some manipulations, a governing equation for the vorticity field

$$\partial_t \boldsymbol{\omega} + \mathbf{u} \cdot \nabla \boldsymbol{\omega} = \boldsymbol{\omega} \cdot \nabla \mathbf{u}, \tag{1.3}$$

usually called the Helmholtz equation.

In a 2D flow, the vorticity is perpendicular to the plane of motion, and therefore equations (1.3) reduce to the advection equation

$$\frac{D\boldsymbol{\omega}}{Dt} := \partial_t \boldsymbol{\omega} + \mathbf{u} \cdot \nabla \boldsymbol{\omega} = 0, \tag{1.4}$$

where the material derivative $D\boldsymbol{\omega}/Dt$ represents the variation of the vorticity field along particle trajectories. The simpler equations (1.4) preserve the enstrophy of the flow, defined as $\Omega = \frac{1}{2}\int |\boldsymbol{\omega}|^2 d\mathbf{x}$, half of L^2 norm of the vorticity field. Taking advantage of this fact, one proves global-in-time regularity for the solutions of the 2D equations [76, 64].

However, due to the presence of the nontrivial nonlinear term on the left hand side of (1.3), the 3D case establishes a totally different scenario. The flow does not preserve the enstrophy anymore and, thus, the arguments of global regularity used in the 2D equations are no longer valid.

1.1 The Blowup Problem for the 3D Incompressible Euler Equations

The question about the regularity of 3D Euler solutions is partially answered by the many local-in-time existence theorems, e.g., [58, 28, 50, 74]. They assert that if the velocity field is initially smooth at $t = 0$, then it remains smooth up to a certain finite time $T > 0$ depending on the initial data. However, we know little about the solution beyond this particular instant. What could prevent the solution from being smoothly extended for all times is the development of a singularity in finite time, i.e., the loss of regularity at a certain instant $t_b > 0$. Such event is called *finite-time blowup*, or simply *blowup*, and the time instant t_b at which it occurs is the blowup time. The name is motivated by the fact that some norm, related to the degree of regularity of the field, becomes arbitrarily large as t approaches t_b.

The central problem we address in this thesis is:

The blowup problem for the Euler equations: *does there exist a regular solution of the 3D incompressible Euler equations* (1.2) *that becomes singular (blows up) in a finite time?*[1]

The existence of blowup in incompressible ideal flow is a long-standing open problem both for physics and mathematics. On the physical side, such blowup is anticipated by Kolmogorov's theory of developed turbulence [36], predicting that the vorticity field diverges at small scales as $\delta\omega \sim \ell^{-2/3}$, while the time of energy transfer between the integral and viscous scales remains finite in the inviscid limit, $\nu \to 0$. In this context, the blowup would reveal an efficient mechanism of energy transfer from large to small scales.

From the mathematical perspective, the inkling of blowup comes from the quadratic nonlinearity of the Euler equations. This may be informally argued as follows [6]. Considering the Helmholtz equation (1.3), if we assume the velocity gradient and the vorticity (which is actually its antisymmetric part) to be identified

$$\nabla \mathbf{u} \approx \boldsymbol{\omega}, \tag{1.5}$$

one obtains (disregarding the distinction between scalars, vectors and tensors) a quadratic differential equation

$$\frac{D\omega}{Dt} \approx \omega^2 \tag{1.6}$$

for the vorticity in a Lagrangian framework (i.e., along particle trajectories).

Equation (1.6) is the common textbook example of an ordinary differential equation that blows up in finite time. Its solution for initial data $\omega(t=0) = \omega_0 > 0$ is given by

$$\omega(t) = \frac{1}{t_b - t}, \quad t_b = \omega_0^{-1}, \tag{1.7}$$

which grows to infinity as t approaches the blowup time t_b, i.e.,

$$\omega(t) \to \infty, \text{ as } t \to t_b. \tag{1.8}$$

[1]The blowup problem for the Euler equations is also formulated in the presence of physical boundaries [32, 54], which is a related but different question. Similar open problems on finite-time singularities, which are fundamental for the understanding of physical behavior, exist across many other fields such as natural convection [64], geostrophic motion [69, 24], magnetohydrodynamics [9], plasma physics [39, 4] and, of course, general relativity [22].

Although we cannot make the above argument rigorous, it displays some subtle features about the blowup problem that happen to be true. In the 1980s, Beale, Kato and Majda published the famous blowup criterion:

Theorem 1.1 (Beale-Kato-Majda Theorem [5])**.** *Let* $\mathbf{u}$ *be a smooth solution of the Euler equations and suppose there is a time* t_b *such that the solution cannot be smoothly continued to* $t = t_b$*; assume that* t_b *is the first such time. Then*

$$\int_0^{t_b} ||\boldsymbol{\omega}(\cdot, s)||_\infty ds = \infty, \tag{1.9}$$

and in particular

$$\limsup_{t \uparrow t_b} ||\boldsymbol{\omega}(\cdot, t)||_\infty = \infty. \tag{1.10}$$

The Beale-Kato-Majda Theorem has two important consequences. First, it shows that the maximum vorticity controls the blowup. Second, if the maximum vorticity diverges with the assymptotic behavior

$$||\boldsymbol{\omega}(\cdot, t)||_\infty \sim (t_b - t)^{-\beta}, \tag{1.11}$$

then, for the integral (1.9) to diverge, we must necessarily have $\beta \geq 1$. Clearly, from dimensional analysis, we expect the equality to hold, i.e., $\beta = 1$, since the vorticity field has dimension of inverse time. Nevertheless, we remark that Theorem 1.1 is a conditional statement: it characterizes the possible singularities in the Euler equations, but it does not claim them to happen.

With such criterion in hand, it is appealing to look for a plausible singularity formation through numerical simulations. Indeed, the unique quantity that needs to be tracked is the maximum vorticity, while the theorem also constraints how it should behave in the case of blowup. We briefly review the numerical investigations now.

1.1.1 Direct Numerical Simulations

Besides purely mathematical studies, e.g., [5, 18, 73], a crucial role in the blowup analysis is given to direct numerical simulations (DNS)[2]. The chase after numerical evidence of blowup in the 3D incompressible Euler equations has a long history [38]. Most early numerical studies were in favor of blowup, e.g., [71, 52, 42]. But the increase of resolution owing to more powerful computers showed that the growth of small-scale

[2]See also [59] for DNS of the blowup at a physical boundary.

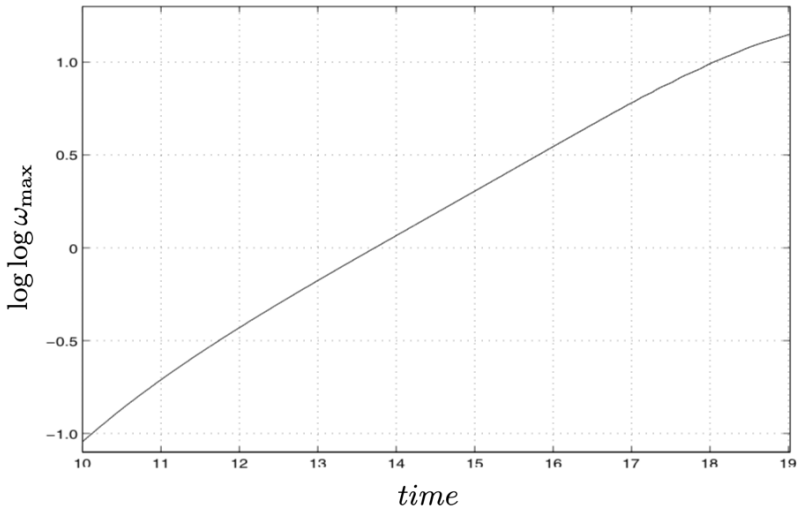

Fig. 1.2 Plot of $\log\log\omega_{\max}$ versus time, obtained from DNS at resolution $1536\times1024\times3072$. The growth is not greater than double exponential for the whole simulation. Figure taken from [46].

structures may be depleted at smaller scales, even though it was demonstrating initially the blowup tendency [47, 41, 46]. This may be explained by the self-organization of the flow into quasi-two-dimensional vorticity structures, a regularizing phenomenon [2] (recall that 2D flows are proved to retain smoothness). Some numerical studies [53, 46] report that the growth of vorticity is not greater than double exponential, which would prevent the blowup to occur if such rate of growth persisted for longer times – see Fig. 1.2.

Figure 1.3 displays the typical picture of DNS results: the growth of vorticity is usually moderate (not greater than 20 times the initial condition), there is no clear tendency of assymptotics, and the solutions are strongly sensitive to perturbations (even to numerical noise), a fact that resembles a chaotic nature [72].

It is fair to say that, now, there is a lack of consensus even on the more probable answer (existence or not) to the blowup problem[3]. It remains an active area of numerical research [53, 12, 56], but computational limitations are still the major obstacle. Indeed, a typical state-of-the-art DNS will not exceed a resolution of 8192^3 node points. This represents a spatial range of approximately 4×10^3 in Fourier space, which appears to be insufficient for the blowup analysis.

[3]In his review, Gibbon [38] gives a score of 9 against 7 for the blowup and no-blowup claims, respectively, from numerical studies reported in literature.

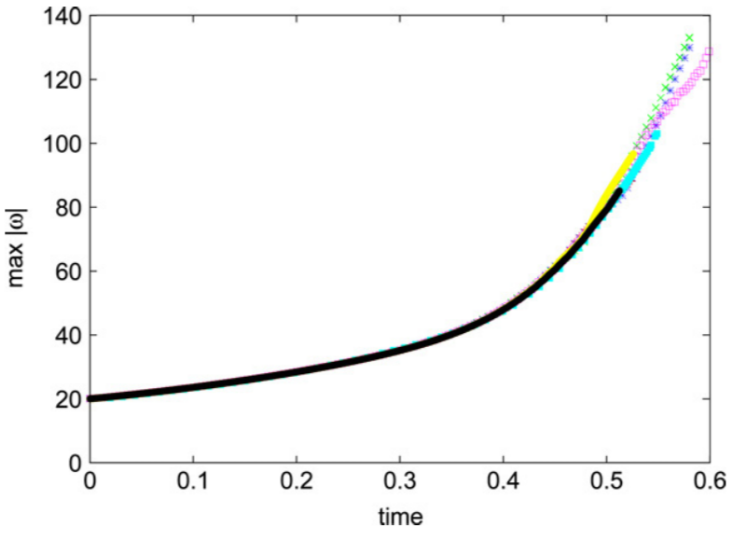

Fig. 1.3 Growth of maximum vorticity for different numerical schemes. Figure taken from [41].

1.1.2 Simplified Models

Numerical limitations of the DNS can be overcome using simplified models [75, 27, 62]. They were developed in lower spatial dimensions, like the Burgers equation [15] and the Constantin-Lax-Majda model [23, 66], or by exploring the cascade ideas in the so-called shell models [40, 65, 60]. Other approaches consider the restriction of the Euler or Navier-Stokes dynamics to a self-similar set of wave vectors, e.g., the reduced wave vector set approximation (REWA) model introduced in [31, 44] and the geometrical formulation proposed in [45].

Despite being rather successful in the study of turbulence [43, 7, 10] and serving as a useful testing ground for mathematical analysis [51, 21], these models fall short of reproducing basic features of Euler's blowup phenomenon. Most of them are one-dimensional models and, thus, lack incompressibility. The Burgers equation is a compressible model and it develops shock singularities, which do not occur in the incompressible Euler flow. Regarding regularity and singularities, shell models are closer to the Burgers equation than the Euler system [63]. The Constantin-Lax-Majda model presents a self-similar blowup, which is prohibited in the Euler solutions [17, 19]. Among the available simplified models, the REWA model is the most structurally similar to the Euler equations, being a three-dimensional like model[4] and presenting

[4]The REWA model fixes a finite number of directions in the 3D Fourier space where the restricted nodes lie.

incompressibility constraint. Nevertheless, it shares with other models a geometric simplicity in its formulation, which prevents all of them from reproducing the observed vorticity structures from full DNS, e.g., two-dimensional depletion.

1.2 Goals and Structure of this Thesis

In the introductory section 1.1, we presented the main question addressed in this thesis — the blowup problem for the 3D incompressible Euler equations. The approaches to this problem and their underlying difficulties can be summarized as follows:

1. *Direct numerical simulations.* The state-of-the-art results display an insufficient spatial resolution, justified by their high computational cost. As a consequence, they established a controversy even about the most probable answer (existence of blowup or not);

2. *Simplified models.* They allow high resolution simulations, but are too simple for the blowup analysis, since they are structurally far from Euler equations and cannot reproduce observed structures from DNS.

In view of this, the goal of this thesis is to formulate a new modelling technique that, when applied to the Euler system, overcomes the above obstacles: it should retain most of the features of the Euler flow, but still allowing a reliable blowup analysis through numerical simulations.

The technique we propose considers the restriction of the Fluid Dynamics equations to a discrete lattice of logarithmically distributed nodes $\mathbb{\Lambda}$ in Fourier space. For these restricted equations to make sense, we need to define calculus and algebraic operations on this new domain, which are especially designed for the resulting simplified models to be structurally identical to the original ones. The main operation is the product between two functions (the nonlinearities of the equations), which should mimic a convolution sum

$$(f * g)(k) \simeq \sum_{\substack{p,q\in\mathbb{\Lambda} \\ k=p+q}} f(p)g(q), \quad k \in \mathbb{\Lambda}, \tag{1.12}$$

coupling triads $k = p + q$ of interacting points on the lattice. Here, the first methodological problem arises, since the logarithmic lattice is not closed under addition, i.e., the sum of two points p and q of the lattice $\mathbb{\Lambda}$ does not necessarily lie again on the lattice. Therefore, our first task is to determine all possible triad interactions $k = p + q$ of points lying on the lattice. This will allow us to obtain every possible product of

form (1.12), providing a classification of all models that may be introduced by our methodology.

Unlike many previous simplified models, the application of our approach to the Euler equations preserves not only the basic symmetries and invariants (energy and helicity) but also a number of fine properties of the Euler flow, such as incompressibility and Kelvin's circulation theorem, in a generalized form, and its solutions correlate with the existing DNS at the respective scales. Furthermore, it allows highly accurate numerical simulations spanning a huge spatial range (up to sixteen orders of magnitude). All these features provide a robust technique for the study of singularities.

This thesis is divided into two parts: in the first one, we formulate the modelling technique on the logarithmic lattice, while in the second, we apply it to the Fluid Dynamics equations. The chapters are organized as follows. In Chapter 2, we define the logarithmic lattices and study their geometry. The main result is the classification of the lattices based on their triad interactions. In Chapter 3, we endow the space of functions on the logarithmic lattice with some operations. The main operation is the product (or convolution sum) between functions. The classification of triads is used here to obtain all possible products on the lattice. Chapter 4 serves as a testing ground: we show that the application of this operational structure on the lattice to the Burgers equation preserves most of its properties and reproduces their known singularities. For specific choices of parameters, the resulting systems are reduced to the known shell models of turbulence. In Chapter 5 we apply our modelling technique to the 3D Euler equations, while in Chapter 6 we use the resulting model for the blowup problem. We conclude with a short summary of the results and discuss possible future developments.

The results reported in Chapters 5 and 6 were published in the article [16] and presented at the conferences

Workshop on Mathematical and Computational Problems of Incompressible Fluid Dynamics. *Chaotic blowup in the 3D incompressible Euler equations on a logarithmic lattice.* IMPA, Rio de Janeiro – RJ, Brazil. August 10-11, 2018;

ICMC Summer Meeting on Differential Equations. *Fluid Dynamics on the logarithmic lattice and singularities of Euler flow.* São Carlos – SP, Brazil. February 4-6, 2019.

Part I

The Triad Structure of Logarithmic Lattices

Chapter 2

Logarithmic Lattices

In this chapter, we study the geometry of logarithmic lattices, the domain on which the dynamical models shall be defined. Logarithmic lattices were first applied in the so-called shell models of turbulence in the 1970s [25]. Here we provide a new systematic study of these lattices as an independent mathematical object. The main result is their classification with respect to triad interactions $k = p + q$. This classification shall be used in the next chapter to formulate products (convolution sums) between functions defined on lattices.

Given a real number $\lambda > 1$, the **logarithmic lattice** with spacing λ is the set $\mathbb{\Lambda} := \{\pm\lambda^n\}_{n\in\mathbb{Z}}$ consisting of positive and negative integer powers of λ.

This set has two main properties. First, $\mathbb{\Lambda}$ is scale-invariant, i.e., $\mathbb{\Lambda} = \sigma\lambda^n\mathbb{\Lambda}$ for any sign $\sigma = \pm 1$ and any integer n. This is fundamental for the study of hydrodynamic turbulence, which is characterized by statistical scale-invariance. Secondly, the points λ^n grow geometrically with n. Thus, with only a few nodes we span a large range of scales. However, the logarithmic lattice is not closed under addition, which imposes a strong restriction to its applications. This is a question we address now.

A **triad interaction** on the logarithmic lattice $\mathbb{\Lambda}$ at the point $k \in \mathbb{\Lambda}$ is an ordered triple

$$\mathfrak{t} = (k, p, q), \text{ with } p, q \in \mathbb{\Lambda}, \text{ such that } k = p + q. \tag{2.1}$$

The set of all triad interactions on $\mathbb{\Lambda}$ at $k \in \mathbb{\Lambda}$ shall be denoted by $\mathcal{T}(\mathbb{\Lambda}; k)$, while the collection of all triads on $\mathbb{\Lambda}$ is the union $\mathcal{T}(\mathbb{\Lambda}) := \cup_{k\in\mathbb{\Lambda}}\mathcal{T}(\mathbb{\Lambda}; k)$. The lattice is called **reducible** if it can be split into two nonempty disjoint subsets $\mathbb{\Lambda} = \mathbb{\Lambda}_1 \cup \mathbb{\Lambda}_2$, $\mathbb{\Lambda}_1 \cap \mathbb{\Lambda}_2 = \varnothing$, such that $\mathcal{T}(\mathbb{\Lambda}) = \mathcal{T}(\mathbb{\Lambda}_1) \cup \mathcal{T}(\mathbb{\Lambda}_2)$. The subsets $\mathbb{\Lambda}_1$ and $\mathbb{\Lambda}_2$ are not coupled by triads, giving rise to two disconnected lattices. A logarithmic lattice which is not reducible is

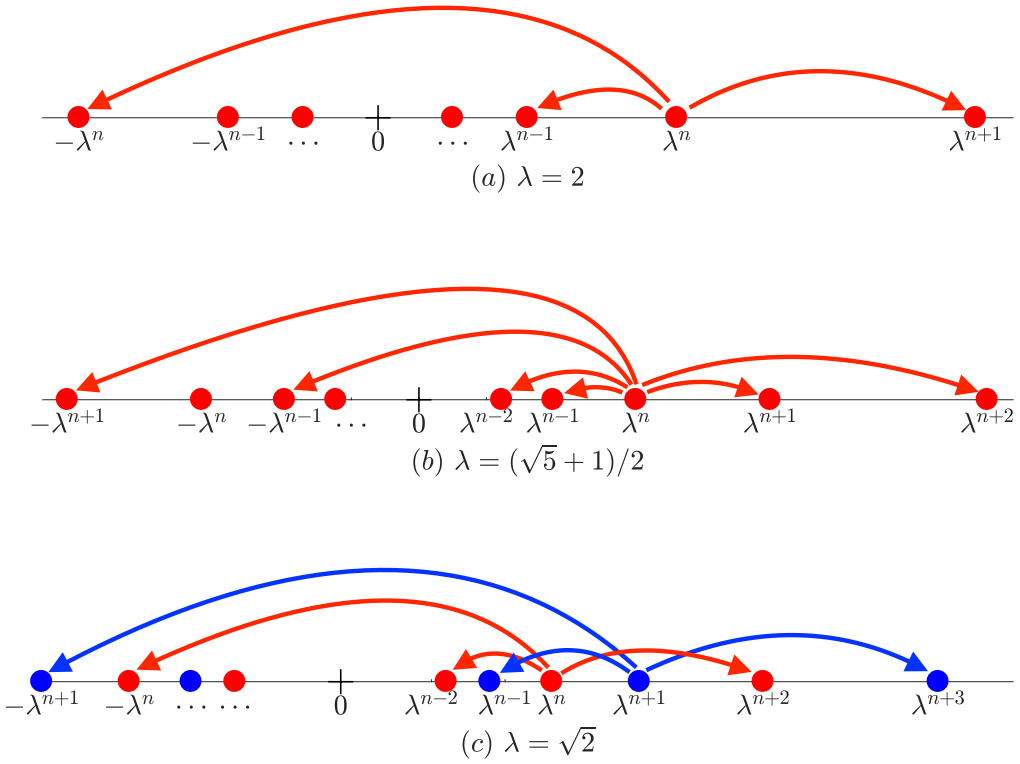

Fig. 2.1 Triad interactions on logarithmic lattices with different spacings λ.

called an **irreducible** lattice. An irreducible lattice has a triad at every $k \in \mathbb{\Lambda}$, i.e.,

$$\mathcal{T}(\mathbb{\Lambda}; k) \neq \varnothing, \quad \text{for every } k \in \mathbb{\Lambda}. \tag{2.2}$$

We say that the logarithmic lattice $\mathbb{\Lambda}$ **interacts in triads** if it has the property (2.2).

We are interested in a twofold task: *i*) to determine which spacings λ generate irreducible lattices and *ii*) to classify all triad interactions $\mathcal{T}(\mathbb{\Lambda})$ of such lattices.

Before giving some examples, let us show that every triad interaction at $k \in \mathbb{\Lambda}$ is the scaling by k of a triad at the unity. This reduces the problem of triad classification to the determination of the triads at this unique point. We claim that for every $k \in \mathbb{\Lambda}$

$$\mathcal{T}(\mathbb{\Lambda}; k) = \{(k, kp, kq);\ (1, p, q) \in \mathcal{T}(\mathbb{\Lambda}; 1)\} \tag{2.3}$$

Indeed, using the fact that the logarithmic lattice is closed under multiplication and division, given a triad decomposition of the unity $\mathfrak{t} = (1, p, q)$, the product $k\mathfrak{t} = (k, kp, kq)$ is a triad at k. Conversely, given $\mathfrak{t} = (k, p, q)$, we have $\mathfrak{t} = k\widetilde{\mathfrak{t}}$, where $\widetilde{\mathfrak{t}} = (1, p/k, q/k)$ is a triad decomposition of the unity.

Thus, in order to determine every triad interaction on $\mathbb{\Lambda}$, it suffices to characterize the set $\mathcal{T}(\mathbb{\Lambda};1)$, i.e., to find every

$$\mathfrak{t}_i = (1, \mu_i, \eta_i), \text{ with } \mu_i, \eta_i \in \mathbb{\Lambda}, \text{ such that } 1 = \mu_i + \eta_i. \tag{2.4}$$

By doing so, every triad at $k \in \mathbb{\Lambda}$ has the form $k\mathfrak{t}_i = (k, \mu_i k, \eta_i k)$.

A logarithmic lattice $\mathbb{\Lambda}$ interacts in triads only for certain spacings λ. If, for example, $\lambda = 2$, then every point $k \in \mathbb{\Lambda}$ interacts with its immediate neighbors and all three triad decompositions of the unity (2.4) are enumerated in the table 2.1 – see Fig. 2.1(a).

Table 2.1 Triads at the unity $1 = \mu_i + \eta_i$ when $\lambda = 2$.

i	1	2	3
μ_i	2	-1	1/2
η_i	-1	2	1/2

The number of interactions can be improved by considering $\lambda = (\sqrt{5}+1)/2$, the golden mean, which satisfies the relation $1 = \lambda^2 - \lambda$. The triads at the unity are obtained from permutations and rescalings of such identity, providing the richer sample of triads in table 2.2. In this case, each point interacts with its two immediate neighbors – see Fig. 2.1(b).

Table 2.2 Triads at the unity $1 = \mu_i + \eta_i$ when $\lambda = (\sqrt{5}+1)/2$.

i	1	2	3	4	5	6
μ_i	λ^2	$-\lambda$	λ	$-\lambda^{-1}$	λ^{-2}	λ^{-1}
η_i	$-\lambda$	λ^2	$-\lambda^{-1}$	λ	λ^{-1}	λ^{-2}

Because immediate neighbors are coupled, these are two examples of irreducible lattices. On the other hand, if $\lambda = \sqrt{2}$, the triads at the unity are given by table 2.3 and now the nodes are coupled two by two. Therefore, the lattice is reducible into $\mathbb{\Lambda} = \mathbb{\Lambda}_1 \cup \mathbb{\Lambda}_2$, where $\mathbb{\Lambda}_1$ takes the even powers of λ and $\mathbb{\Lambda}_2$ the odd ones – see Fig. 2.1(c).

Table 2.3 Triads at the unity $1 = \mu_i + \eta_i$ when $\lambda = \sqrt{2}$.

i	1	2	3
μ_i	λ^2	-1	λ^{-2}
η_i	-1	λ^2	λ^{-2}

From the above examples, depending on the spacing λ we obtain logarithmic lattices with broader or narrower interacting bands. For practical purposes, we are not interested in the limit $\lambda \to 1$, which represents the collapse of the lattice to a unique point. Therefore, we shall classify all irreducible lattices whose spacing is bounded from below as $\lambda \geq \lambda_0$ by some $\lambda_0 > 1$ sufficiently small[1].

The main result of this chapter is the characterization of irreducible logarithmic lattices with respect to their triad interactions, given by the following theorem.

Theorem 2.1. *Let Λ be an irreducible logarithmic lattice with spacing $\lambda \geq 1.05$. Then, Λ corresponds to one of the following three cases:*

(i) $\lambda = 2$*, and all triads at the unity are given in table 2.1;*

(ii) $\lambda = \lambda_* := \frac{\sqrt[3]{9+\sqrt{69}}+\sqrt[3]{9-\sqrt{69}}}{2^{1/3}3^{2/3}} \approx 1.325$*, the plastic number*[2]*, and all triads at the unity are given in table 2.4;*

Table 2.4 Triads at the unity $1 = \mu_i + \eta_i$ when $\lambda = \lambda_*$.

i	1	2	3	4	5	6	7	8	9	10	11	12
μ_i	λ^3	$-\lambda$	λ^2	$-\lambda^{-1}$	λ^{-3}	λ^{-2}	λ^5	$-\lambda^4$	λ	$-\lambda^{-4}$	λ^{-5}	λ^{-1}
η_i	$-\lambda$	λ^3	$-\lambda^{-1}$	λ^2	λ^{-2}	λ^{-3}	$-\lambda^4$	λ^5	$-\lambda^{-4}$	λ	λ^{-1}	λ^{-5}

(iii) otherwise, the spacing λ satisfies $1 = \lambda^b - \lambda^a$ for some integers $0 < a < b \leq 65$, $(a, b) \neq (1, 3), (4, 5)$, with greatest common divisor $\gcd(a, b) = 1$, and all triads at the unity are given in table 2.5.

Table 2.5 Triads at the unity $1 = \mu_i + \eta_i$ when λ satisfies $1 = \lambda^b - \lambda^a$ for integers $0 \leq a < b$.

i	1	2	3	4	5	6
μ_i	λ^b	$-\lambda^a$	λ^{b-a}	$-\lambda^{-a}$	λ^{-b}	λ^{a-b}
η_i	$-\lambda^a$	λ^b	$-\lambda^{-a}$	λ^{b-a}	λ^{a-b}	λ^{-b}

Proof. Let us show that given integers $0 \leq a < b$, there exists a unique logarithmic lattice Λ allowing triad interactions, whose spacing λ satisfies $1 = \lambda^b - \lambda^a$.

[1]The bound $\lambda \geq \lambda_0$ by some $\lambda_0 > 1$ is essential for the proof, otherwise it becomes equivalent to finding the intersection of algebraic curves with arbitrary degrees, which is a difficult problem in algebraic geometry [70].

[2]Cf. [1].

We start proving this assertion by showing that the trinomial $p(x) = x^b - x^a - 1$ has a unique real root λ greater than unity. Indeed, the case $a = 0$ gives $\lambda = 2^{1/b}$. If $0 < a < b$, existence of such a root is a consequence of the Intermediate Value Theorem, since $p(1) = -1$ and $\lim_{x\to+\infty} p(x) = +\infty$, while uniqueness follows from the strictly positive derivative $p'(x) = bx^{b-1} - ax^{a-1} > 0$ for all $x > 1$.

Next, let $\mathbb{\Lambda}$ be the (unique) logarithmic lattice whose spacing $\lambda > 1$ satisfies $1 = \lambda^b - \lambda^a$. By rescaling this identity and permuting its terms, we obtain the triad interactions in table 2.5, which reduces to table 2.1 in the case $a = 0$. Observe that these triads represent only local interactions and the role of the integers a and b is precisely to state which neighbors are coupled.

Conversely, if the logarithmic lattice $\mathbb{\Lambda}$ interacts in triads, then its spacing $\lambda > 1$ satisfies $1 = \lambda^b - \lambda^a$ for some integers $0 \leq a < b$. Indeed, from identity (2.3), if the lattice interacts in triads, then there exist $\mu, \eta \in \mathbb{\Lambda}$ summing up to unity $1 = \mu + \eta$. These points have the form $\mu = \sigma\lambda^b, \eta = \tau\lambda^a$, with $\sigma, \tau \in \{\pm 1\}$ and $a, b \in \mathbb{Z}$. We may assume without loss of generality that $0 \leq a \leq b$; rescale the identity by some integer power of λ, if necessary. For two points of this form to be a decomposition of unity, we must necessarily have $\sigma = 1$, $\tau = -1$, while a and b must satisfy $0 \leq a < b$.

To determine every possible triad interaction in a lattice we need to find all pair of integers $0 \leq a < b$ for which the given spacing λ satisfies $1 = \lambda^b - \lambda^a$. With this information in hand, all triad interactions are given by table 2.5 for each pair (a, b). This problem is reformulated as a system of trinomial equations. Consider two trinomials given by

$$p_j(x) = x^{b_j} - x^{a_j} - 1, \quad 0 \leq a_j < b_j, \ j = 1, 2. \tag{2.5}$$

For which distinct integers a_1, a_2, b_1, b_2 the system $p_1 = p_2 = 0$ has a real root $\lambda > 1$?

Now we use the hypothesis $\lambda \geq 1.05$ to bound the degree of such polynomials. This will simplify the difficult problem of finding the intersection of algebraic curves with arbitrary degree to a case of large but bounded degrees. Namely, we claim that for $\lambda \geq 1.05$ satisfying $1 = \lambda^b - \lambda^a$ with integers $0 \leq a < b$ we must have $b \leq 65$. We shall prove the contrapositive in three steps.

First, let us consider two spacings λ_1 and λ_2 satisfying $1 = \lambda_1^b - \lambda_1^a$ and $1 = \lambda_2^b - \lambda_2^c$ with $0 \leq a \leq c \leq b$. Then we have $\lambda_1 \leq \lambda_2$. This follows from the fact that, if we define the polynomials $p_1(x) = x^b - x^a - 1$ and $p_2(x) = x^b - x^c - 1$, we have that each one has a (unique) root greater than unity, both polynomials are strictly increasing in $[1, \infty)$ and $p_2 \leq p_1$ in this interval. Therefore, if we fix the higher exponent b of the identity $1 = \lambda^b - \lambda^a$, the spacing λ is maximized when $a = b - 1$.

Next, we show that the spacings λ_b satisfying $1 = \lambda_b^b - \lambda_b^{b-1}$ form a decreasing sequence with respect to b. To prove this, we apply the same argument as above. Consider the polynomials $p_b(x) = x^b - x^{b-1} - 1$. For $x \geq \lambda_b > 1$ we have $p_b(x) \leq xp_b(x) = x^{b+1} - x^b - x < x^{b+1} - x^b - 1 = p_{b+1}(x)$. Therefore, since these polynomials are strictly increasing for $x > 1$, we have $\lambda_{b+1} < \lambda_b$, so we conclude that the λ_b is a decreasing sequence as $b \to \infty$.

Finally, computing the roots λ_b for each b numerically, one verifies that if $b \geq 65$, then $\lambda_b < 1.05$ and, in view of the above statements, every λ satisfying $1 = \lambda^b - \lambda^a$ with $0 \leq a < b$ and $b \geq 65$ is also bounded by the same value, $\lambda < 1.05$.

With bounded degrees $b_j \leq 65$, the trinomial system (2.5) can be evaluated in a finite number of cases. Numerical analysis shows that the only solution for this problem is the family of roots $\lambda_k := \lambda_*^{1/k}$ satisfying both (and only) the trinomial identities

$$1 = \lambda_k^{3k} - \lambda_k^k, \quad \text{and } 1 = \lambda_k^{5k} - \lambda_k^{4k}. \tag{2.6}$$

We have characterized all nontrivial logarithmic lattices. They must be one of the three cases: *i*) $\lambda = 2^{1/b}$ for some integer $b > 0$; the triads at unity are given by table 2.1; *ii*) $\lambda = \lambda_*^{1/k}$ for some integer $k > 0$; we need to combine the triads from table 2.5 for both $(a, b) = (k, 3k)$ and $(a, b) = (4k, 5k)$ and they are depicted in table 2.4; *iii*) λ satisfies $1 = \lambda^b - \lambda^a$ for some integers $0 < a < b < 65$, $(a, b) \neq (k, 3k), (4k, 5k)$ for all integer $k > 0$, and the triads are enumerated in table 2.5. See, e.g., Fig. 2.1(b) for the case $a = 1$ and $b = 2$.

Lastly, we want to extract from these lattices the irreducible ones. Given a lattice with spacing λ satisfying $1 = \lambda^b - \lambda^a$ for some integers $0 \leq a < b$, if the greatest common divisor $\gcd(a, b) = k$, then the lattice can be reduced into k uncoupled lattices. Thus, the condition for irreducibility is mathematically translated to $\gcd(a, b) = 1$. Applying this criterion to each of the three cases, we obtain the desired classification of irreducible lattices. □

We say that the logarithmic lattice $\mathbb{\Lambda}$ is **associative** at $k \in \mathbb{\Lambda}$ if for every $p, q, r \in \mathbb{\Lambda}$ such that $k = p + q + r$ we have $p + q, q + r \in \mathbb{\Lambda}$. When this occurs, the sums in parentheses in the identity $(p + q) + r = p + (q + r)$ lie on the lattice.

We show next that when sums are restricted to the logarithmic lattice then the lattice is nowhere associative. This property will be related with the lack of associativity of products in the next chapter.

Theorem 2.2. *The logarithmic lattices described in Theorem 2.1 are nowhere associative.*

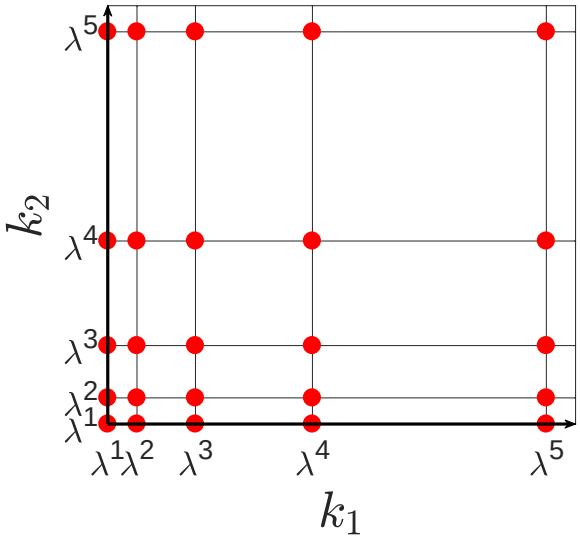

Fig. 2.2 A two-dimensional logarithmic lattice $\mathbb{\Lambda}^2$ with spacing λ.

Proof. In view of identity (2.3), it suffices to show that the lattice $\mathbb{\Lambda}$ is not associative at the unity.

We have shown in the proof of Theorem 2.1 that if the lattice interacts in triads, then there are integers $0 \le a < b$ such that the spacing λ satisfies $1 = \lambda^b - \lambda^a$.

Take $p = \lambda^{2b}$, $q = -\lambda^{a+b}$ and $r = -\lambda^a$. Then

$$p + q + r = \lambda^{2b} - \lambda^{a+b} - \lambda^a = \lambda^b(\lambda^b - \lambda^a) - \lambda^a = \lambda^b - \lambda^a = 1.$$

Let us show that $q + r = -(1 + \lambda^b)\lambda^a \notin \mathbb{\Lambda}$, which will prove the theorem. We claim that the factor $1 + \lambda^b \notin \mathbb{\Lambda}$. Indeed, suppose that $1 + \lambda^b \in \mathbb{\Lambda}$. In this case, $1 + \lambda^b = \lambda^m$ for some integer $m > b$. It follows that λ is a solution of the trinomial system (2.5) with $a_1 = a$, $b_1 = b$, $a_2 = b$ and $b_2 = m$. However, we already proved that such solutions do not exist, see Eq. (2.6), leading to a contradiction. □

The above results for a one-dimensional logarithmic lattice can be extended to higher dimensions.

The **n-dimensional logarithmic lattice** with spacing $\lambda > 1$ is given by the cartesian power $\mathbb{\Lambda}^n = \mathbb{\Lambda} \times \cdots \times \mathbb{\Lambda}$ (n factors) – see Fig. 2.2 for the two-dimensional picture. A point $\mathbf{k} \in \mathbb{\Lambda}^n$ of the n-dimensional logarithmic lattice is an n-tuple $\mathbf{k} = (k_1, \ldots, k_n)$ where each component k_j lies on $\mathbb{\Lambda}$. An ordered triple $\mathbf{t} = (\mathbf{k}, \mathbf{p}, \mathbf{q})$ of points from the lattice $\mathbf{k}, \mathbf{p}, \mathbf{q} \in \mathbb{\Lambda}^n$ is a triad interaction if each component $k_j = p_j + q_j$ is a triad interaction on $\mathbb{\Lambda}$. Thus all irreducible lattices $\mathbb{\Lambda}^n$ are given by the spacings λ listed in

Theorem 2.1 and all triads are combinations of the one-dimensional triads for each component.

The notion of associativity on the logarithmic lattice also extends naturally to higher dimensions and it follows that the n-dimensional lattice is associative at a point $\mathbf{k} \in \mathbb{\Lambda}^n$ if the one-dimensional lattice $\mathbb{\Lambda}$ is associative at each component k_j. For this reason, $\mathbb{\Lambda}^n$ is nowhere associative, just as in the one-dimensional case.

Chapter 3

Functions on a Logarithmic Lattice

The main purpose of this chapter is to endow the space of functions on the logarithmic lattice with calculus and algebraic operations that mimic the correspondent operations between continuous functions, defined on the whole Euclidean space. By tracking their essential properties, this will allow to formulate, in the next chapters, simplified models structurally identical to the original fluid dynamical equations, sharing most of their underlying attributes, e.g., symmetries and conserved quantities.

Let $\mathbb{\Lambda}$ be an irreducible logarithmic lattice with spacing λ and consider $k \in \mathbb{\Lambda}$, which we interpret as a wave number in Fourier space. Let us consider complex valued functions $f(k) \in \mathbb{C}$ of the wave number k and impose the reality condition

$$f(-k) = \overline{f(k)} \tag{3.1}$$

where the bar denotes complex conjugation. This condition is motivated by the same property of the Fourier transform of a real valued function. Thus, f is analogous to the Fourier transform of a real function. The space of functions f defined on the logarithmic lattice $\mathbb{\Lambda}$ and satisfying (3.1) shall be denoted by $\mathcal{F}(\mathbb{\Lambda})$.

A function $f(k)$ on the lattice may be interpreted in several ways. For instance, consider a real function $F : \mathbb{R} \to \mathbb{R}$ on the real line and fix a positive lattice point $k \in \mathbb{\Lambda}$. By considering the Fourier transform

$$\hat{F}(k') = \int_{\mathbb{R}} F(x) e^{-ik'x} dx, \quad k' \in \mathbb{R}, \tag{3.2}$$

one may associate the discrete value $f(k)$ on the logarithmic lattice with the average of $\hat{F}$ over the interval $[k, \lambda k]$, that is

$$f(k) \simeq \frac{1}{\lambda k - k} \int_k^{\lambda k} \hat{F}(k')dk', \quad k \in \mathbb{\Lambda}. \tag{3.3}$$

In this interpretation, F may represent some physical variable. Then f maintains the physical dimension of $\hat{F}$, providing dimensional coherence to the modelling.

The value $f(k)$ could also be understood as the integration of $\hat{F}$ in the interval $[k, \lambda k]$ without the prefactor:

$$f(k) \simeq \int_k^{\lambda k} \hat{F}(k')dk', \quad k \in \mathbb{\Lambda}. \tag{3.4}$$

In this second approach, the dimensionality of f and $\hat{F}$ differ by the spatial dimension.

These two interpretations are summarized in a single formula

$$f(k) \simeq \frac{1}{|\lambda k - k|^\alpha} \int_k^{\lambda k} \hat{F}(k')dk', \quad k \in \mathbb{\Lambda}, \tag{3.5}$$

where the **scaling exponent** α takes unit value in the average definition (3.3) and zero in the integration approach (3.4). If we define the rescaled function $\delta_\lambda F(x) = F(x/\lambda)$, one may check directly from definition (3.5) and from the Fourier transform property $\widehat{(\delta_\lambda F)}(k) = \lambda F(\lambda k)$ that the corresponding rescaled function on the logarithmic lattice is

$$\delta_\lambda f(k) = \lambda^\alpha f(\lambda k). \tag{3.6}$$

Therefore, the model on the logarithmic lattice scales with the λ^α prefactor.

In what follows, we construct an operational structure for the space $\mathcal{F}(\mathbb{\Lambda})$, aiming to capture the essential differential and algebraic properties of continuous models.

Given two functions f and g in $\mathcal{F}(\mathbb{\Lambda})$, we define their **inner product** as

$$(f, g) := \sum_{k \in \mathbb{\Lambda}} |k|^\alpha f(k)\overline{g(k)}. \tag{3.7}$$

This definition mimics the standard functional product

$$\int f(x)g(x)dx = \int \hat{f}(k)\overline{\hat{g}(k)}dk$$

for continuous real functions, which is the average of the product fg. The factor $|k|^\alpha$ stands for the volume of integration for the lattice model with scaling exponent α.

Using (3.6) and replacing k by λk in (3.7), yields the scaling property

$$(f,g) = \sum_{k\in\mathbb{\Lambda}} |k|^\alpha f(k)\overline{g(k)} = \sum_{k\in\mathbb{\Lambda}} |\lambda k|^\alpha f(\lambda k)\overline{g(\lambda k)}$$
$$= \lambda^{-\alpha} \sum_{k\in\mathbb{\Lambda}} |k|^\alpha \lambda^\alpha f(\lambda k)\overline{\lambda^\alpha g(\lambda k)} = \lambda^{-\alpha}(\delta_\lambda f, \delta_\lambda g). \quad (3.8)$$

Again, if α equals unity, then the inner product (3.7) maintains the expected physical dimension, since after the scaling the functions by λ, their mean value decreases by a λ factor. Just like the standard functional product of real functions, expression (3.7) is also real valued. Indeed, using the reality condition (3.1) one may rewrite equation (3.7) as

$$(f,g) = 2\mathrm{Re}\left(\sum_{\substack{k\in\mathbb{\Lambda}\\ k>0}} |k|^\alpha f(k)\overline{g(k)}\right). \quad (3.9)$$

Since we are working with Fourier-space representation, we define the space derivative ∂_x by the Fourier factor,

$$\partial_x f(k) = ikf(k), \quad (3.10)$$

where i is the imaginary unit. Clearly, higher order derivatives are powers of the Fourier factors. This notion of differentiability on the lattice retains some important calculus identities, like integration by parts

$$(\partial_x f, g) = -(f, \partial_x g), \quad (3.11)$$

which follows from the fact that the inner product (3.7) couples $f(k)$ and $\overline{g(k)} = g(-k)$.

We next define the product of two functions on the logarithmic lattice, which in Fourier space is understood as a convolution.

A **product on the logarithmic lattice** (or simply a **product**), represented by $*$, is a binary operation on $\mathcal{F}(\mathbb{\Lambda})$ satisfying, for any functions $f, g, h \in \mathcal{F}(\mathbb{\Lambda})$ and any numbers $\gamma, \xi \in \mathbb{R}$, the following properties:

(P.1) (Reality condition) $(f * g)(-k) = \overline{(f * g)(k)}$;

(P.2) (Commutativity) $f * g = g * f$;

(P.3) (Bilinearity) $(f + \gamma g) * h = f * h + \gamma(g * h)$;

(P.4) (Translation invariance) $\tau_\xi(f * g) = \tau_\xi f * \tau_\xi g$, where $\tau_\xi f(k) = e^{-ik\xi} f(k)$ is the translation of f by ξ;

(P.5) (Scaling invariance) $\delta_\lambda(f * g) = \delta_\lambda f * \delta_\lambda g$, where $\delta_\lambda f$ is the rescaling of f by λ given by (3.6);

(P.6) (Parity) $P(f * g) = Pf * Pg$, where $Pf(k) = f(-k)$ is the reflection of f with respect to the vertical axis;

(P.7) (Associativity in average) $(f * g, h) = (f, g * h)$;

(P.8) (Leibniz rule) $\partial_x(f * g) = \partial_x f * g + f * \partial_x g$.

The required properties for the product are chosen in order to mimic a common (pointwise) product of real functions on the real line, or, equivalently, a convolution operation in Fourier space. The reality condition *(P.1)* is a closure property. Commutativity *(P.2)*, bilinearity *(P.3)*, translation invariance *(P.4)* and parity *(P.6)* are natural properties of the pointwise product, such as scaling invariance *(P.5)*, although this last property in our case is restricted to the logarithmic lattice, and therefore given in discrete form $k \mapsto \lambda k$. The Leibniz rule *(P.8)* is responsible for the coupling of triads. As we shall see below, since the logarithmic lattice is nowhere associative, see Theorem 2.2, we cannot demand the product to be associative. Nevertheless, we require the weaker property of associativity in average *(P.7)*. This property also justifies the use of the following notation. We define the **product average** of two functions as

$$\langle f * g \rangle := (f, g) \tag{3.12}$$

and the product average of three functions as the common value

$$\langle f * g * h \rangle := (f * g, h) = (f, g * h). \tag{3.13}$$

Indeed, from the definitions of inner product and product on the logarithmic lattice, they mimic the average values $\int f(x)g(x)dx$ and $\int f(x)g(x)h(x)dx$, respectively. We remark that higher order product averages are not well-defined, due to the lack of associativity.

We shall see in the next chapters that these properties provide an algebraic structure similar to the one in the original equations of Fluid Dynamics. As a result, the new simplified models will present the same symetries and preserve most of the invariants.

We establish now the general form of the product on the one-dimensional lattice. Later, it will be generalized to higher dimensions. By introducing the norm

$$||f||_1 := \sum_{k \in \mathbb{\Lambda}} |k|^\alpha |f(k)|, \tag{3.14}$$

we define the space of absolutely summable functions, consisting of functions f with finite norm (3.14).

Theorem 3.1. *Let $\mathbb{\Lambda}$ be one of the logarithmic lattices described in Theorem 2.1. Then, the following operations define products on $\mathcal{F}(\mathbb{\Lambda})$:*

(i) For $\lambda = 2$,

$$(f * g)(k) = c|k|^{\alpha}[f(2k)\overline{g(k)} + \overline{f(k)}g(2k) + 4^{-\alpha}f(2^{-1}k)g(2^{-1}k)], \tag{3.15}$$

where $c \in \mathbb{R}$ is an arbitrary real parameter;

(ii) For $\lambda = \lambda_* := \frac{\sqrt[3]{9+\sqrt{69}}+\sqrt[3]{9-\sqrt{69}}}{2^{1/3}3^{2/3}}$,

$$\begin{aligned}(f * g)(k) = c|k|^{\alpha}\{&\lambda^{2\alpha}[f(\lambda^3 k)\overline{g(\lambda k)} &+ \overline{f(\lambda k)}g(\lambda^3 k)]\\ &+f(\lambda^2 k)\overline{g(\lambda^{-1}k)} &+ \overline{f(\lambda^{-1}k)}g(\lambda^2 k)\\ &+\lambda^{-4\alpha}[f(\lambda^{-3}k)g(\lambda^{-2}k) &+ f(\lambda^{-2}k)g(\lambda^{-3}k)]\}\\ +d|k|^{\alpha}\{&\lambda^{8\alpha}[f(\lambda^5 k)\overline{g(\lambda^4 k)} &+ \overline{f(\lambda^4 k)}g(\lambda^5 k)]\\ &+f(\lambda k)\overline{g(\lambda^{-4}k)} &+ \overline{f(\lambda^{-4}k)}g(\lambda k)\\ &+\lambda^{-2\alpha}[f(\lambda^{-5}k)g(\lambda^{-1}k) &+ f(\lambda^{-1}k)g(\lambda^{-5}k)]\},\end{aligned} \tag{3.16}$$

where $c, d \in \mathbb{R}$ are arbitrary real parameters;

(iii) Otherwise, $1 = \lambda^b - \lambda^a$ and

$$\begin{aligned}(f * g)(k) = c|k|^{\alpha}\{&\lambda^{2a\alpha}[f(\lambda^b k)\overline{g(\lambda^a k)} &+ \overline{f(\lambda^a k)}g(\lambda^b k)]\\ &+f(\lambda^{b-a}k)\overline{g(\lambda^{-a}k)} &+ \overline{f(\lambda^{-a}k)}g(\lambda^{b-a}k)\\ &+\lambda^{-2(b-a)\alpha}[f(\lambda^{-b}k)g(\lambda^{a-b}k) &+ f(\lambda^{a-b}k)g(\lambda^{-b}k)]\}\end{aligned} \tag{3.17}$$

where $c \in \mathbb{R}$ is an arbitrary real parameter.

Additionally, if f and g are absolutely summable, then also is $f * g$.

Conversely, these are the most general products in the space of absolutely summable functions.

Proof. Properties *(P.1)* to *(P.8)* for the products (3.15)–(3.17) can be verified directly by substitution.

Let us show that the product $f * g$ of two absolutely summable functions f and g is again an absolutely summable function. We prove it below using the known Generalized Young Inequality on measure spaces.

Give the logarithmic lattice $\mathbb{\Lambda}$ the measure m pointwisely defined by

$$m(\{k\}) = |k|^{\alpha}, \quad k \in \mathbb{\Lambda}.$$

In this case, the norm (3.14) is written as the integral

$$||f||_1 = \int |f| dm \tag{3.18}$$

The three products depicted in the Theorem have the same structure

$$(f * g)(k) = \sum_{j=1}^{N} c_j |k|^{\alpha} f(\mu_j k) g(\eta_j k), \tag{3.19}$$

where N is the number of terms, c_j are real parameters of the product, μ_j and η_j are nonzero coupling factors.

The Generalized Young Inequality is stated as [35, p.9]: *Let (X, μ) be a σ-finite measure space, and let $p \in [1, \infty]$ and $A > 0$. Suppose that K is a measurable function on $X \times X$ such that*

$$\sup_{x \in X} \int_X |K(x, y)| d\mu(y) \leq A, \quad \sup_{y \in X} \int_X |K(x, y)| d\mu(x) \leq A. \tag{3.20}$$

If $g \in L^p(X)$, then the function Tg defined by

$$Tg(x) = \int_X K(x, y) f(y) d\mu(y) \tag{3.21}$$

is well-defined almost everywhere, it is in $L^p(X)$, and

$$||Tg||_{L^p(X)} \leq A ||g||_{L^p(X)} \tag{3.22}$$

For functions f and g defined on the euclidean space $\mathbb{R}^n$, the known Young's Inequality $||f * g||_{L^p(\mathbb{R}^n)} \leq ||f||_{L^1(\mathbb{R}^n)} ||g||_{L^p(\mathbb{R}^n)}$ for the usual convolution follows from (3.22) by taking $K(x, y) = f(x - y)$. However, we cannot do this on our domain, since the difference of points from the logarithmic lattice does not necessarily lie on the logarithmic lattice. A slight modification of this kernel is necessary.

Define the kernel $K : \mathbb{\Lambda} \times \mathbb{\Lambda} \to \mathbb{C}$

$$K(k, q) = \begin{cases} \frac{c_j}{|\eta_j|^{\alpha}} f(\mu_j k), & \text{if } q = \eta_j k, \ j = 1, \ldots, N; \\ 0, & \text{otherwise.} \end{cases}$$

Then,

$$\int K(k,q)g(q)dm(q) = \sum_{q\in\mathbb{\Lambda}} |q|^\alpha K(k,q)g(q) = \sum_{j=1}^{N} |\eta_j k|^\alpha \frac{c_j}{|\eta_j|^\alpha} f(\mu_j k)g(\eta_j k) = (f*g)(k),$$

where we used (3.19) in the last equality.

Additionally, by setting $C = \max_{j=1,\dots,N} \frac{|c_j|}{|\mu_j|^\alpha}$ and using the norm (3.18), one obtains

$$\begin{aligned}\int |K(k,q)|dm(q) &= \sum_{q\in\mathbb{\Lambda}} |q|^\alpha |K(k,q)| = \sum_{j=1}^{N} |\eta_j k|^\alpha \frac{|c_j|}{|\eta_j|^\alpha} |f(\mu_j k)| \\ &= \sum_{j=1}^{N} |\mu_j k|^\alpha \frac{|c_j|}{|\mu_j|^\alpha} |f(\mu_j k)| \leq C \sum_{j=1}^{N} |\mu_j k|^\alpha |f(\mu_j k)| \leq C||f||_1.\end{aligned}$$

for every $k \in \mathbb{\Lambda}$, from which

$$\sup_{k\in\mathbb{\Lambda}} \int |K(k,q)|dm(q) \leq C||f||_1.$$

Following the same steps, one proves the other inequality

$$\sup_{q\in\mathbb{\Lambda}} \int |K(k,q)|dm(k) \leq C||f||_1.$$

The Generalized Young Inequality with $A = C||f||_1$ yields

$$||f*g||_1 \leq C||f||_1||g||_1 < \infty,$$

which shows that $f*g$ is an absolutely summable function.

Let $*$ be a product on the space of absolutely summable functions, here denoted by ℓ^1. The product is a bilinear operator $*:\ \ell^1 \times \ell^1 \to \ell^1$. Its action at two ℓ^1 functions is given by

$$(f*g)(k) = \sum_{p,q\in\mathbb{\Lambda}} c_{kpq} f(p)g(q)$$

where $c_{kpq} \in \mathbb{R}$ are real coefficients independent of f and g.

The Leibniz rule *(P.8)* restricts the sum to triads $k = p+q$. From Theorem 2.1, there is only a finite number N of triads at each k and we can write the triads at k as $k = p_j + q_j$ with $p_j = \mu_j k$ and $q_j = \eta_j k$. As a consequence, the coefficients can be rewritten as $c_{kp_jq_j} = c_j^k$. The scaling invariance *(P.5)* shows that the dependence of coefficients c_j^k on k is given by the volume factor $c_k^j = |k|^\alpha c_j$. Parity *(P.6)* demands the coefficients to be independent on the sign of k. Hence, the product can be rewritten

in the general form (3.19). Finally, commutativity *(P.2)* and associativity in average *(P.7)* define the coefficients c_j.

We skip these elementary but cumbersome calculations which lead to the expressions (3.15)–(3.17) for each lattice spacing. □

Observe that the three products (3.15)–(3.17) have the convolution form (3.19) coupling triads, where the coupling factors μ_j and η_j are given by Theorem 2.1 and the coefficients c_j are given in Theorem 3.1. Particularly, for $\alpha = 0$,

$$(f * g)(k) = \sum_{\substack{p,q \in \mathbb{\Lambda} \\ k=p+q}} f(p)g(q). \tag{3.23}$$

Since all products couple triads in the form (3.23), a direct consequence of the non-asscoativity of the logarithmic lattice expressed in the Theorem 2.2 is the lack of associativity of the products.

Theorem 3.2. *The products described in Theorem 3.1 are not associative:*

$$(f * g) * h \neq f * (g * h). \tag{3.24}$$

Recall that the associativity condition is valid in average. However, since the products are not associative, we cannot extend the definition of product average to more than three factors.

We reinforce also the choice of focusing on irreducible lattices. Because a product always couple triads, in a reducible lattice such product decouples the dynamics into two noninteracting lattices.

Finally, it is possible to generalize the operations between functions introduced in this chapter to higher dimensions. By considering a n-dimensional logarithmic lattice $\mathbb{\Lambda}^n$, the space of functions $f(\mathbf{k})$ of the wave vector $\mathbf{k} \in \mathbb{\Lambda}^n$ satisfying the reality condition (3.1) is denoted by $\mathcal{F}(\mathbb{\Lambda}^n)$. The inner product between two functions $f, g \in \mathcal{F}(\mathbb{\Lambda}^n)$ is defined as

$$(f, g) := \sum_{\mathbf{k} \in \mathbb{\Lambda}^n} |k_1 \dots k_n|^\alpha f(\mathbf{k}) \overline{g(\mathbf{k})}, \tag{3.25}$$

while the partial derivatives are given by the Fourier factors

$$\partial_j f(\mathbf{k}) = i k_j f(\mathbf{k}), \quad j = 1, \dots, n. \tag{3.26}$$

The product on $\mathcal{F}(\mathbb{\Lambda}^n)$ is also a binary operation on this set satisfying properties *(P.1)* to *(P.8)*, except that the parity property *(P.6)* is substituted by the more general isotropy property, which includes rotations and reflections. Namely, by isotropy we imply that the product is invariant under any transformation $\mathbf{R}$ from the group of cube symmetries $\mathsf{O_h}$ (Cf. [55, Sec.93] – this group includes all transformations $(k_1, k_2, k_3) \mapsto (\pm k_{\sigma_1}, \pm k_{\sigma_2}, \pm k_{\sigma_3})$, where σ is a permutation of $(1, 2, 3)$). We express this property as

$$T_{\mathbf{R}}(f * g) = T_{\mathbf{R}} f * T_{\mathbf{R}} g, \tag{3.27}$$

where $T_{\mathbf{R}} f$ is the "rotated" function f by $\mathbf{R} \in \mathsf{O_h}$.

One may apply the same techniques of Theorem 3.1 in order to classificate every product on $\mathcal{F}(\mathbb{\Lambda}^n)$. However, formulation (3.23) gives us a ready-to-use product for any dimension:

$$(f * g)(\mathbf{k}) = \sum_{\substack{\mathbf{p},\mathbf{q} \in \mathbb{\Lambda}^n \\ \mathbf{k}=\mathbf{p}+\mathbf{q}}} f(\mathbf{p}) g(\mathbf{q}). \tag{3.28}$$

We shall apply this product in the Chapter 5 to formulate a model for the 3D Euler equations.

Part II

Fluid Dynamics Models on Logarithmic Lattices

Chapter 4

The Burgers Equation

In this chapter, we present how the operational structure on the logarithmic lattice, introduced in the the first part of this thesis, can be used to formulate simplified models, by considering the Burgers equation in one-dimensional space. This chapter serves as a testing ground before going to the full Euler system. We verify that our methodology not only preserves most of the properties of the Burgers equation but is also capable of reproducing the known singularities of its solutions. We show that, for a specific choice of parameters, the Burgers equation on the logarithmic lattice reduces to a couple of popular shell models of turbulence. Still, our methodology is more general and provides new similar models. Proofs for conservation laws assume that all sums are absolutely convergent. For completing these proofs, one needs to introduce the concept of strong solution, which is out of scope of this thesis.

The Burgers equation is given by

$$\partial_t u + u * \partial_x u = \nu \partial_x^2 u, \tag{4.1}$$

where $\nu \geq 0$ is the viscosity. In physical space, $u = u(x,t)$ with $x \in \mathbb{R}$, the star product corresponds to the usual pointwise multiplication and ∂_x is the spatial derivative. On the other hand, in Fourier-space representation $u = u(k,t)$, the derivative ∂_x is given by the Fourier factor $\partial_x = ik$, while the star denotes a convolution.

Equation (4.1) also makes sense on a logarithmic lattice, when by $*$ we understand a product introduced in Chapter 3.

Independently of the concrete structure of the product, the lattice model (4.1) retains important properties of the continuous Burgers equation, like its symmetry to the physical space translations by a real number $a \in \mathbb{R}$, defined as $u(k) \mapsto e^{-iak}u(k)$, and the conservation of the inviscid ($\nu = 0$) invariants, proved in the following theorem.

Theorem 4.1. *If $u(k,t)$ is a solution of the inviscid ($\nu = 0$) Burgers equation* (4.1)*, then the energy*

$$E(t) := \frac{1}{2}\langle u * u \rangle, \tag{4.2}$$

and the third order moment

$$M(t) := \langle u * u * u \rangle \tag{4.3}$$

are conserved in time.

Proof. Recall that, by the definitions of product averages (3.12) and (3.13), the energy and the third order moment are given by $E = (u, u)$ and $M = (u * u, u) = (u, u * u)$, respectively.

For the energy, taking the time derivative and substituting the equation (4.1), one obtains

$$\frac{dE}{dt} = (\partial_t u, u) = -(u * \partial_x u, u).$$

On the other hand, using successively the Leibniz rule *(P.8)* together with commutativity *(P.2)*, integration by parts (3.11), and associativity in average *(P.7)*, we have

$$-(u * \partial_x u, u) = -\frac{1}{2}(\partial_x (u * u), u) = \frac{1}{2}(u * u, \partial_x u) = \frac{1}{2}(u * \partial_x u, u).$$

It follows that $(u * \partial_x u, u) = 0$, from which $dE/dt = 0$.

For the third order moment, using the associativity in average *(P.7)* and substituting the Burgers equation, one may write

$$\frac{dM}{dt} = 3(u * u, \partial_t u) = -3(u * u, u * \partial_x u)$$

With similar manipulations of the product properties, one obtains

$$\begin{aligned} -3(u * u, u * \partial_x u) &= -\frac{3}{2}(u * u, \partial_x (u * u)) = \\ &= \frac{3}{2}(\partial_x (u * u), u * u) = 3(u * \partial_x u, u * u) = 3(u * u, u * \partial_x u), \end{aligned}$$

from which $(u * u, u * \partial_x u) = 0$ and hence we have also conservation of the moment M. □

The conservation of energy is a property of the shell models of turbulence [10, 26], while the conservation of the third order moment is related to a Hamiltonian structure in the Sabra shell model [61]. Recall from Chapter 3 that higher order moments, e.g.

$\langle u * u * u * u \rangle$, are not well defined due to the lack of associativity in the products – see Theorem 3.2.

One can also make sense of conservation of momentum for the Burgers equation. Consider the continuity equation

$$\partial_t \rho + \partial_x(\rho * u) = 0, \tag{4.4}$$

where ρ is interpreted as the fluid density. The total momentum is defined as the cross-correlation

$$P(t) := \langle \rho * u \rangle, \tag{4.5}$$

which is proved to be conserved in time in the following theorem.

Theorem 4.2. *Let $u(k,t)$ be a solution of the inviscid ($\nu = 0$) Burgers equation* (4.1) *and let $\rho(k,t)$ be a solution of the continuity equation* (4.4)*. Then, the momentum* (4.5) *is conserved in time.*

Proof. Taking the time derivative of (4.5), one obtains two terms

$$\frac{dP}{dt} = (\partial_t \rho, u) + (\rho, \partial_t u),$$

which we treat separately.

For the first term, we substitute the continuity equation (4.4) and apply successively associativity in average *(P.7)*, integration by parts (3.11) and Leibniz rule *(P.8)*:

$$\begin{aligned}(\partial_t \rho, u) &= -(u * \partial_x \rho, u) - (\rho * \partial_x u, u) = -(\partial_x \rho, u * u) - (\rho, u * \partial_x u) \\ &= 2(\rho, u * \partial_x u)) - (\rho, u * \partial_x u) = (\rho, u * \partial_x u).\end{aligned}$$

For the second term, just substitute the Burgers equation (4.1) to obatin

$$(\rho, \partial_t u) = -(\rho, u * \partial_x u).$$

Summing the two contributions, we conclude that $dP/dt = 0$ and the momentum is conserved in time. □

Theorem 4.2 shows that the logarithmic model for the Burgers equation conserves an infinite number of invariants. Indeed, a solution $u(t)$ preserves the cross-correlation (4.5) for every solution $\rho(t)$ of equation (4.4).

Depending on the concrete nature of the product given by Theorem 3.1 presented in Chapter 3, we have different models, as we present now.

4.1 Burgers Equation on Logarithmic Lattices and Shell Models of Turbulence

We show in this section that popular shell models of turbulence are obtained from the one-dimensional Burgers equation by applying our methodology.

First let us take $\lambda = 2$ and consider the product (3.15). The Burgers equation (4.1) takes the form

$$\partial_t u(k) = -\frac{1}{2} cik|k|^\alpha \left[2u(2k)\overline{u(k)} + 4^{-\alpha} u^2\left(\frac{k}{2}\right)\right] - \nu k^2 u(k). \tag{4.6}$$

Let us choose $\alpha = 0$ and $c = 2$. Define the geometric progression

$$k_n := \lambda^n, \quad n \in \mathbb{Z} \tag{4.7}$$

and consider purely imaginary solutions of type

$$u(\pm k_n) = \pm i u_n, \quad \text{for } u_n \in \mathbb{R}. \tag{4.8}$$

Note that Eq. (4.8) is a property of the Fourier transform for any odd function in physical space. Then, the equation (4.6) taken at $k = k_n$ reduces to the form

$$\dot{u}_n = k_n u_{n-1}^2 - k_{n+1} u_{n+1} u_n - \nu_n u_n, \tag{4.9}$$

where we have introduced the viscosities $\nu_n = \nu k_n^2$. This system is known as the Desnyansky-Novikov (DN) shell model [25], also called dyadic model.

For the next example, take $\lambda = (\sqrt{5}+1)/2$, the golden mean, which satisfies $1 = \lambda^2 - \lambda$ and consider the product (3.17) with $a = 1$, $b = 2$, $\alpha = 0$ and $c = -\lambda$ expanded as

$$\begin{aligned}(u * v)(k) = -\lambda[&u(\lambda^2 k)v(-\lambda k) + u(-\lambda k)v(\lambda^2 k) + \\ &+ u(\lambda k)v(-\lambda^{-1}k) + u(-\lambda^{-1}k)v(\lambda k) + \\ &+ u(\lambda^{-2}k)v(\lambda^{-1}k) + u(\lambda^{-1}k)v(\lambda^{-2}k)].\end{aligned} \tag{4.10}$$

With the product (4.10), the Burgers equation (4.1) becomes

$$\partial_t u(k) = i\lambda k[u(\lambda^2 k)\overline{u(\lambda k)} + u(\lambda k)\overline{u(\lambda^{-1}k)} + u(\lambda^{-2}k)u(\lambda^{-1}k)] - \nu k^2 u(k). \tag{4.11}$$

By setting $u(k_n) = u_n$ and $u(-k_n) = \overline{u_n}$ with $k_n = \lambda^n$, the equation (4.11) reduces to the form

$$\dot{u}_n = i[k_{n+1}u_{n+2}\overline{u_{n+1}} - (1+d)k_n u_{n+1}\overline{u_{n-1}} - dk_{n-1}u_{n-1}u_{n-2}] - \nu k_n^2 u_n, \tag{4.12}$$

with $d = -\lambda^2$. System (4.12) is the Sabra shell model [60].

Besides the energy (4.2), the Sabra model (4.12) has one more inviscid quadratic invariant of the form $I = \sum_{n\in\mathbb{Z}} d^{-n}|u_n|^2$. However, this invariant has no analogue for the Burgers equation. In studies of hydrodynamic turbulence, it was interpreted as the enstrophy for $d > 0$ (sign definite invariant) and as helicity for $d < 0$ (not sign-definite invariant).

4.2 Blowup and Shock Solutions

Let us consider the inviscid Burgers equation on the logarithmic lattice of spacing $\lambda = 2$ with constant forcing. Taking Eq. (4.6) with $\nu = 0$, $c = 4$ and $\alpha = 1$, we write our system as

$$\partial_t u(k) = -ik|k|\left[\frac{1}{2}u^2\left(\frac{k}{2}\right) + 4u(2k)\overline{u(k)}\right] + f(k). \tag{4.13}$$

Considering again the geometric progression (4.7) and purely imaginary solutions of form (4.8), system (4.13) can be rewritten as

$$\dot{u}_n = k_n^2\left[\frac{1}{2}u_{n-1}^2 - 4u_{n+1}u_n\right] + f_n \tag{4.14}$$

where we have introduced the forces $f(\pm k_n) = \pm i f_n$ with $f_n \in \mathbb{R}$. For the force, we take the Kronecker delta $f_n = \delta_n^1$, which is equal to one for $n = 1$ and zero otherwise. The initial conditions are set to zero. We provide no perturbations on the nodes $k = \lambda^n, n < 1$. In this case, from the governing equation, $u_n \equiv 0$ for $n < 1$ and all $t \geq 0$ and, therefore, the dynamics is restricted to the nodes k_n with $n \geq 1$ and the boundary condition $u_0 = 0$.

The model (4.13) is integrated numerically with a finite but large number of nodes $N = 60$, thus covering the scale range $2^N \sim 10^{18}$. The truncation error is kept below 10^{-20} for the whole simulation, providing an accurate numerical analysis. The solution blows up as t approaches the blowup time $t_b \approx 0.34543415$, developing a power law $|u(k)| \sim |k|^{-\xi}$ with $\xi \approx 1.19$ – see Fig. 4.1. The scaling is very close to the known

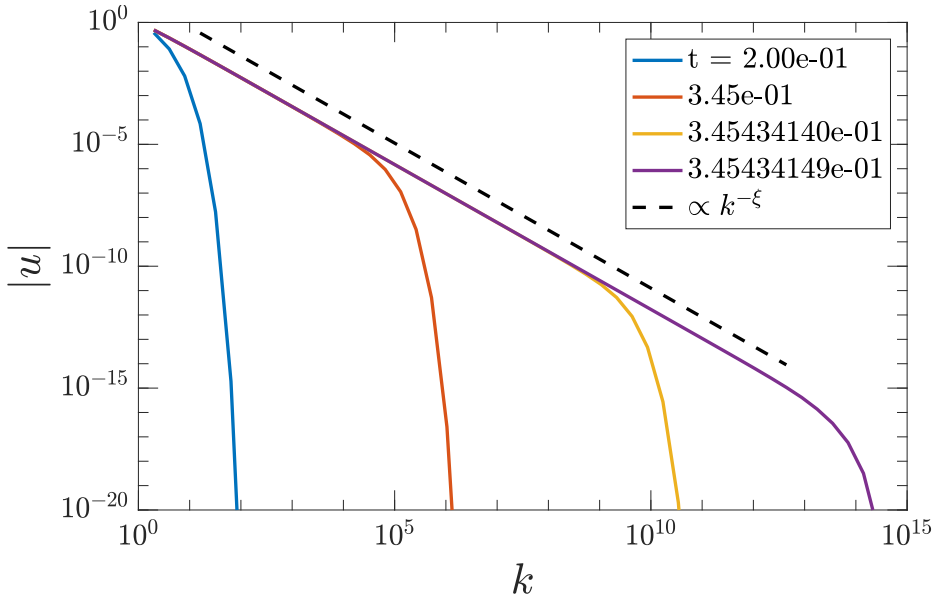

Fig. 4.1 Time evolution for the spectrum $|u(k)|$ as t approaches the blowup time $t_b \approx 0.34543415$, developing a power-law assymptotics $|u(k)| \sim |k|^{-\xi}$ with exponent $\xi \approx 1.19$.

blowup assymptotics for the continuous Burgers equation $u(x) \sim -x^{1/3}$, which in Fourier space becomes $u(k) \sim k^{-4/3}$.

Model (4.13) may be regularized by introducing the viscous term $-\nu k^2 u(k)$ on the right hand side with finite but small viscosity $\nu > 0$. This system reduces to the form

$$\dot{u}_n = k_n^2 \left[\frac{1}{2} u_{n-1}^2 - 4 u_{n+1} u_n\right] - \nu k^2 u_n + f_n, \tag{4.15}$$

analogous to (4.14). In this case, the simulation can be extended beyond the blowup time t_b, from which a transition occurs on the spectrum steepness: the solution assumes an assymptotic power-law scaling $|u(k)| \sim |k|^{-1}$ on the intermediate (inertial) range of wave numbers $k \lesssim 10^4$ and it drops down in the dissipation range $k \gtrsim 10^4$ – see Fig. 4.2. The dissipation range is shifted towards larger k as $\nu \to 0$. One may check by substitution that

$$u(k) = ik^{-1} \tag{4.16}$$

is a fixed-point solution of the inviscid model (4.13). On the real line, the function (4.16) is the Fourier transform of a discontinuous (shock) solution $u(x) = -\frac{1}{2}\text{sign}(x)$ for the Burgers equation. Thus, our lattice model demonstrates the blowup followed by the formation of a shock solution.

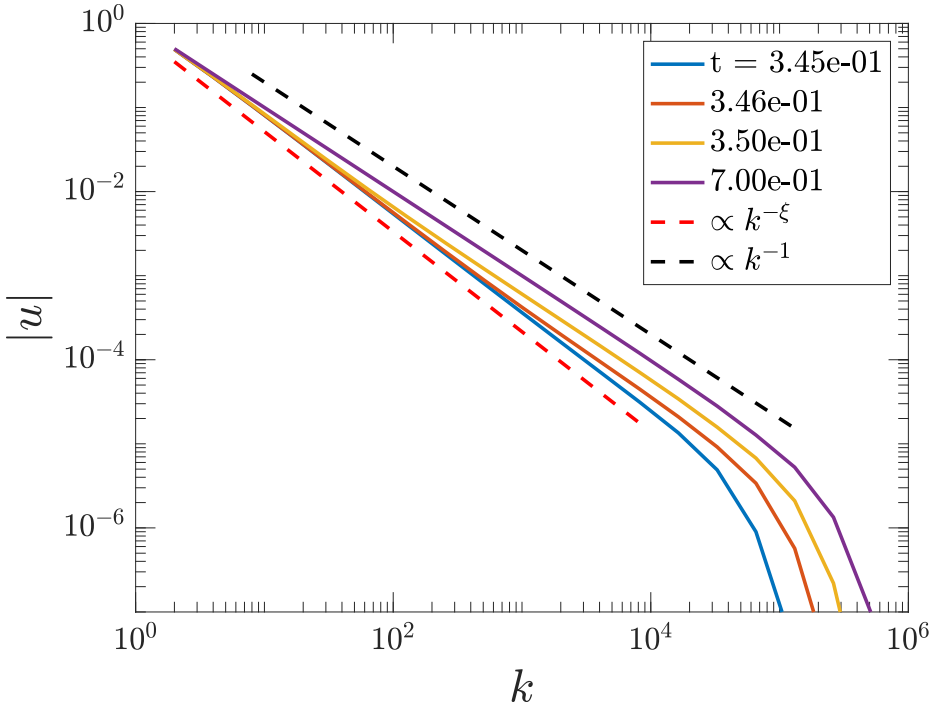

Fig. 4.2 Transition from the blowup assymptotics $|u(k)| \sim |k|^{-\xi}$, with $\xi \approx 1.19$, developed up to the blowup time $t_b \approx 0.345$, to a shock solution $|u(k)| \sim |k|^{-1}$, obtained from viscous regularization with small viscosity, $\nu = 10^{-5}$.

Chapter 5

The 3D Incompressible Euler Equations

In this chapter, we apply our methodology to the 3D incompressible Euler equations.

Let $\mathbb{\Lambda}^3$ be a three-dimensional irreducible logarithmic lattice with spacing λ. In our simplified model, we represent the velocity field as a function $\mathbf{u}(\mathbf{k}, t) = (u_1, u_2, u_3) \in \mathbb{C}^3$ of the wave vector $\mathbf{k} \in \mathbb{\Lambda}^3$ and time $t \in \mathbb{R}$. Thus, at each lattice point, $\mathbf{u}$ stands for the corresponding velocity in Fourier space. Similarly, we define the scalar function $p(\mathbf{k})$ representing the pressure. All functions are supposed to satisfy the reality condition: $u_i(-\mathbf{k}) = \overline{u_i(\mathbf{k})}$. For the governing equations, we use the exact form of 3D incompressible Euler equations

$$\partial_t u_i + u_j * \partial_j u_i = -\partial_i p, \quad \partial_j u_j = 0, \tag{5.1}$$

which are now considered on the logarithmic lattice, with some product $*$ introduced in Chapter 3; here and below repeated indices imply the summation.

The proposed model retains most of the properties of the continuous Euler equations, which rely only upon the structure of the equations and elementary operations on the logarithmic lattice enumerated in Chapter 3. These include the basic symmetry groups.

Theorem 5.1 (Symmetry groups of the Euler equations on the logarithmic lattice)**.** *Let* $\mathbf{u}(\mathbf{k}, t)$ *be a solution of the Euler equations* (5.1)*. Then the following transformations also yield solutions:*

(S.1) (Time translations) $\mathbf{u}^\tau(\mathbf{k}, t) = \mathbf{u}(\mathbf{k}, t + \tau)$*, for any number* $\tau \in \mathbb{R}$*;*

(S.2) (Space translations) $\mathbf{u}^{\boldsymbol{\xi}}(\mathbf{k}, t) = e^{-i\mathbf{k}\cdot\boldsymbol{\xi}}\mathbf{u}(\mathbf{k}, t)$*, for any vector* $\boldsymbol{\xi} \in \mathbb{R}^n$*;*

(S.3) (Isotropy) $\mathbf{u}^{\mathbf{R}}(\mathbf{k},t) = \mathbf{R}^T\mathbf{u}(\mathbf{Rk},t)$, *for any transformation* $\mathbf{R}$ *from the group of cube symmetries* $\mathsf{O_h}$ *(Cf. [55, Sec.93]);*

(S.4) (Scale invariance) $\mathbf{u}^{\lambda,\tau}(\mathbf{k},t) = \lambda^{\alpha+1}\tau\mathbf{u}\left(\lambda\mathbf{k},\tau t\right)$, *for any nonzero* τ, *where* λ *is the lattice spacing and* α *is the scaling exponent* (3.5).

The symmetries of the Euler equations on the logarithmic lattice are the same as those for the continuous model, except that isotropy *(S.3)* and scaling invariance *(S.4)* are given in discrete form.

Model (5.1) also preserves the same invariants as the continuous Euler equations. Let us show this first for the energy and helicity. Like in Chapter 4, the proofs for the conservation laws are formal: they assume that all sums are convergent and can be manipulated. For these proofs to be rigorous, one needs to define the proper function spaces, on which the variables and their derivatives are summable up to a certain order. However, this is beyond the scope of this thesis.

Theorem 5.2 (Conservation of energy and helicity)**.** *Let* $\mathbf{u}(\mathbf{k},t)$ *be a solution of the Euler equations* (5.1)*. Then the energy*

$$E(t) := \frac{1}{2}\langle u_i * u_i\rangle \tag{5.2}$$

and the helicity

$$H(t) := \langle u_i * \omega_i\rangle, \tag{5.3}$$

where $\boldsymbol{\omega} := \nabla \times \mathbf{u}$ *is the vorticity, are conserved in time.*

Proof. Taking the energy as an example, let us show how the proof can be written using the basic operations defined on the logarithmic lattice, following the standard approach of Fluid Dynamics. Using the Euler equations (5.1), we obtain

$$\begin{aligned}\frac{dE}{dt} &= \frac{d}{dt}\left[\frac{1}{2}(u_i,u_i)\right] = (u_i,\partial_t u_i)\\ &= -(u_i,\partial_i p) - (u_i, u_j * \partial_j u_i).\end{aligned}$$

The pressure term vanishes owing to the incompressibility condition as

$$(u_i,\partial_i p) = -(\partial_i u_i, p) = 0,$$

where the first relation is obtained from the integration by parts (3.11). In the inertial term, using commutativity of the product *(P.2)*, the Leibniz rule *(P.8)* and the

associativity in average *(P.7)*, one obtains

$$(u_i, u_j * \partial_j u_i) = (u_i * \partial_j u_i, u_j) = \frac{1}{2}(\partial_j (u_i * u_i), u_j).$$

After integration by parts, this term vanishes due to the incompressibility condition.

Conservation of helicity can be proved following a similar line of derivations. □

One can also make sense of Kelvin's circulation theorem in the three-dimensional system (5.1). It is related to the conservation of cross-correlation $\Gamma := \langle u_i * h_i \rangle$ for an arbitrary "frozen-into-fluid" divergence-free field $\mathbf{h}(\mathbf{k}, t) = (h_1, h_2, h_3)$ satisfying the equations

$$\begin{aligned} \partial_t h_i + u_j * \partial_j h_i - h_j * \partial_j u_i = 0, \quad i = 1, 2, 3 \\ \partial_j h_j = 0. \end{aligned} \tag{5.4}$$

Theorem 5.3 (Kelvin's Theorem)**.** *Let* $\mathbf{u}(\mathbf{k}, t)$ *be a solution of the three-dimensional Euler equations* (5.1) *and consider a "frozen-into-fluid" divergence-free field* $\mathbf{h}(\mathbf{k}, t)$ *satisfying equations* (5.4)*. Then the cross-correlation*

$$\Gamma(t) = \langle u_i * h_i \rangle \tag{5.5}$$

is conserved in time.

Since equations (5.4) are satisfied by the vorticity field $\boldsymbol{\omega}$, the proof for conservation of the cross-correlation $\Gamma = \langle u_i * h_i \rangle$ follows the same steps as for conservation of helicity $H = \langle u_i * \omega_i \rangle$.

In the continuous formulation, the circulation around a closed material contour $\mathbf{C}(s, t)$ in physical space (s is the arc length parameter) is given by the cross-correlation Γ with the field [77]

$$\mathbf{h}(\mathbf{x}, t) = \oint \frac{\partial \mathbf{C}(s, t)}{\partial s} \, \delta^3(\mathbf{x} - \mathbf{C}(s, t)) \, ds, \tag{5.6}$$

where δ^3 is the 3D Dirac delta-function. This field satisfies the continuous analogue to equations (5.4) in the distributional sense. Thus, the conservation of Γ defined as (5.5) yields exactly the circulation in Kelvin's theorem. For the lattice model, its conservation provides an infinite number of circulation invariants: the cross-correlation Γ is conserved for any solution of system (5.4).

Chapter 6

Chaotic Blowup in the 3D Incompressible Euler Equations

In this chapter, we use the lattice model of the 3D incompressible Euler equations introduced in the Chapter 5 for the study of the blowup problem in this system. We start by formulating the numerical model and presenting the simulations. Next, we explain the blowup as a chaotic wave in a renormalized system. We conlude with a comparison between our results and those from the existing DNS.

6.1 Numerical Model and Simulations

Let $\mathbb{\Lambda}^3$ be the 3D logarithmic lattice with spacing $\lambda = (\sqrt{5}+1)/2$, the golden mean, which satisfies $1 = \lambda^2 - \lambda$. All triads on this lattice are obtained from combinations of the one-dimensional triads given by Theorem 2.1. This provides 216 interactions at each lattice point. We consider the product on the logarithmic lattice introduced in Chapter 3,

$$(f * g)(\mathbf{k}) = \sum_{\substack{\mathbf{p},\mathbf{q}\in\mathbb{\Lambda}^3 \\ \mathbf{k}=\mathbf{p}+\mathbf{q}}} f(\mathbf{p})g(\mathbf{q}). \tag{3.28}$$

The sum in equation (3.28) has 216 terms, the number of triads at each node point.

For numerical simulations, we used the Euler equations in vorticity formulation

$$\partial_t \omega_i + u_j * \partial_j \omega_i - \omega_j * \partial_j u_i = 0, \tag{6.1}$$

where $\mathbf{u} = \mathrm{rot}^{-1}\boldsymbol{\omega} = i\mathbf{k}\times\boldsymbol{\omega}/|\mathbf{k}|^2$; here and below repeated indices imply the summation.

Aiming for the blowup study, we consider initial conditions limited to large scales. They are explicitly given below in terms of velocities. Nonzero components are limited to scales $\lambda \le |k_{1,2,3}| \le \lambda^3$ and taken in the form

$$u_j(\mathbf{k}) = \frac{|\epsilon_{jmn}|}{2} k_m k_n e^{i\theta_j(\mathbf{k})-|\mathbf{k}|}, \quad \text{for} \quad j = 1, 2. \tag{6.2}$$

Here ϵ_{jmn} is the Levi-Civita permutation symbol and the phases θ_j are given by

$$\begin{aligned} \theta_j(\mathbf{k}) &= \mathrm{sgn}(k_1)\alpha_j + \mathrm{sgn}(k_2)\beta_j + \mathrm{sgn}(k_3)\delta_j \\ &\quad + \mathrm{sgn}(k_1 k_2 k_3)\gamma_j \end{aligned} \tag{6.3}$$

with the constants $(\alpha_1, \beta_1, \delta_1, \gamma_1) = (1, -7, 13, -3)/4$ and $(\alpha_2, \beta_2, \delta_2, \gamma_2) = (-1, -3, 11, 7)/4$. The third component of velocity is uniquely defined by the incompressibility condition.

Equations (6.1) are integrated with double-precision using the fourth-order Runge-Kutta-Fehlberg adaptive scheme. The local error, relative to $\omega_{\max}(t)$, was kept below 10^{-10}. Since only a finite number of modes $n = 1, \ldots, N$ can be simulated, the infinite-dimensional nature of the problem was tracked very accurately by using the following adaptive scheme in the simulation. At each time step, we computed the enstrophy $\Omega = \frac{1}{2}(\omega_i, \omega_i)$ of the modes with wavenumbers $|\mathbf{k}| \ge K_{\max}/\lambda$, where $K_{\max}$ is the largest wavenumber in each direction of the lattice. This quantity estimates the enstrophy error due to mode truncation, and it was kept extremely small, below 10^{-20}, during the whole simulation. Every time the threshold of 10^{-20} was reached we increased the number of nodes in each direction by five, i.e., multiplying $K_{\max}$ by λ^5. Together, this provided the remarkably high accuracy of numerical results. We stopped the simulation with $N = 80$, thus, covering the scale range of $\lambda^N \sim 10^{17}$ with the total of 13180 time steps. The energy was conserved at all times with the relative error below 3.8×10^{-10}.

Figures 6.1(a) and 6.1(b) analyze the temporal evolution of the maximum vorticity $\omega_{\max}(t) = \max_{\mathbf{k}\in\mathbb{\Lambda}^3} |\boldsymbol{\omega}(\mathbf{k}, t)|$ and the corresponding wave number $k_{\max}(t) = |\mathbf{k}|$. The Beale-Kato-Majda theorem [5] (whose proof for our model is identical to the continuous case) states that the blowup of the solution at finite time t_b requires that the integral $\int_0^t \omega_{\max}(t)dt$ diverges as $t \to t_b$. In particular, this implies that the growth of maximum vorticity must be at least as fast as $\omega_{\max}(t) \gtrsim (t_b - t)^{-1}$. This dependence is readily confirmed in Fig. 6.1(a) providing the blowup time $t_b = 15.870 \pm 0.001$. Furthermore, Fig. 6.1(b) tracks the dependence $\omega_{\max}(t) \sim (t_b - t)^{-1}$ in logarithmic coordinates up to the values $\omega_{\max} \sim 10^5$. The same figure demonstrates the power-law dependence $k_{\max}(t) \sim (t_b - t)^{-\gamma}$ with the exponent $\gamma = 2.70 \pm 0.01$, simulated up to extremely small

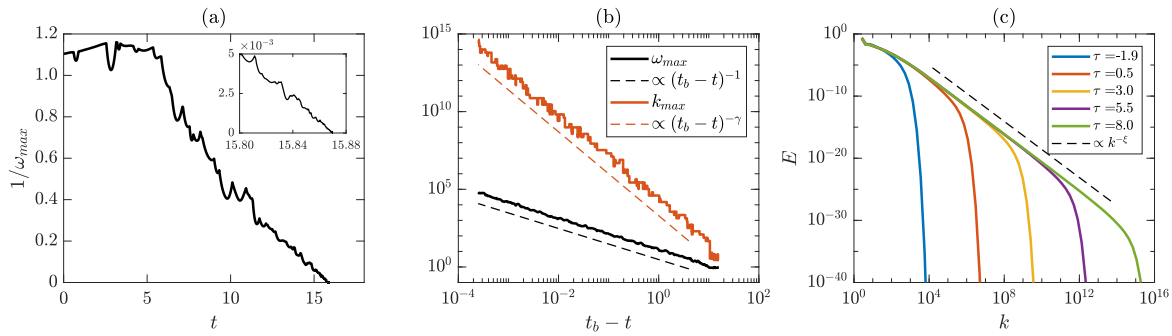

Fig. 6.1 (a) Inverse maximum vorticity, $1/\omega_{\max}$, as a function of time; the inset displays an amplified segment very close to the blowup time $t_b = 15.870$. The graph shows deterministic chaotic oscillations; it is not smooth, because the vorticity maximum jumps between nodes of the 3D lattice with increasing time. (b) Evolution of maximum vorticity in log-scale, demonstrating chaotic oscillations around the power law $\propto (t_b - t)^{-1}$, and wave number $k_{\max}$ corresponding to the vorticity maximum, following in average the power law $(t_b - t)^{-\gamma}$ with $\gamma = 2.70$. (c) The energy spectrum, $E(k) = \frac{1}{2\Delta} \sum_{k \le |\mathbf{p}| < \lambda k} |\mathbf{u}(\mathbf{p})|^2$ with $\Delta = \lambda k - k$, in log-scale at different renormalized times $\tau = -\log(t_b - t)$. As $t \to t_b$ corresponding to $\tau \to \infty$, the spectrum develops the power law $E \propto k^{-\xi}$ with $\xi = 3 - 2/\gamma \approx 2.26$.

physical scales, $\ell \sim 1/k_{\max} \sim 10^{-15}$. Finally, Fig. 6.1(c) shows the development of the power law $E(k) \propto k^{-\xi}$ in the energy spectrum as $t \to t_b$. The exponent can be obtained with the dimensional argument $E \propto \omega_{\max}^2 / k_{\max}^3$, which yields $\xi = 3 - 2/\gamma \approx 2.26$.

6.2 Chaotic Blowup

The observed scaling agrees with the Leray-type [57] self-similar blowup solution $\boldsymbol{\omega}_L(\mathbf{k}, t)$ defined as

$$\boldsymbol{\omega}_L(\mathbf{k}, t) = (t_b - t)^{-1} \mathbf{W}[(t_b - t)^{\gamma} \mathbf{k}]. \tag{6.4}$$

Such a solution, however, cannot describe the blowup in Fig. 6.1, where the maximum vorticity and the corresponding scale $\ell \sim 1/k_{\max}$ have the power-law behavior only in average, with persistent irregular oscillations.

In order to understand the nonstationary blowup dynamics, we perform the change of coordinates

$$\begin{aligned} \widetilde{\boldsymbol{\omega}} &= (t_b - t)\boldsymbol{\omega}, & \eta &= \log |\mathbf{k}|, \\ \mathbf{o} &= \mathbf{k}/|\mathbf{k}|, & \tau &= -\log(t_b - t). \end{aligned} \tag{6.5}$$

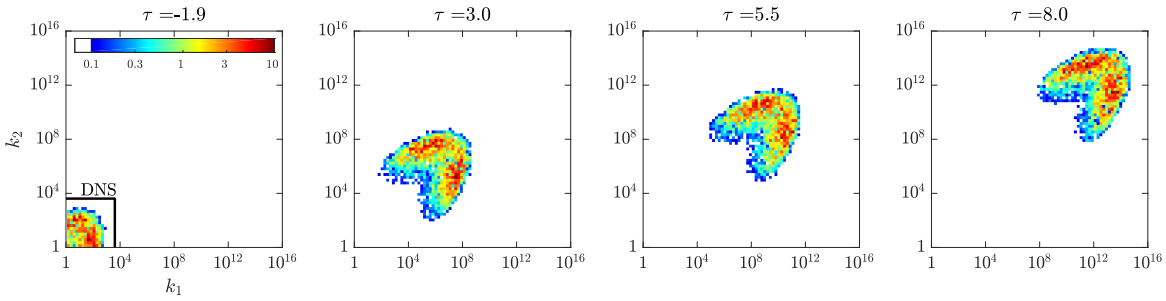

Fig. 6.2 Absolute value of the third component of renormalized vorticity $|\widetilde{\omega}_3|$, as a function of two positive wave numbers $k_1 > 0$ and $k_2 > 0$ (in log scale) at four different instants τ. The third wave number is fixed at the node nearest to $k_3 = e^{\gamma\tau+6} \propto (t_b - t)^{-\gamma}$. Values below 0.1 are plotted in white. In the left figure, the small box bounds the square region $|k_{1,2}| \le 4096$, which would be accessible for the high-accuracy DNS with resolution 8192^3.

This change of coordinates applies similarly in Fourier space $\mathbb{R}^3$ and in our 3D lattice $\mathbb{\Lambda}^3$. With the renormalized variables (6.5), it is convenient to define new differentiation operators as the Fourier factors $\widetilde{\partial}_j = io_j$, where $\mathbf{o} = (o_1, o_2, o_3) = \mathbf{k}/|\mathbf{k}|$ and i is the imaginary unit. Thus, derivatives in the original and in the renormalized variables are related as $\partial_j = e^{\eta}\widetilde{\partial}_j$. Also, the renormalized velocity can be defined as $\widetilde{\mathbf{u}} = (t_b - t)|\mathbf{k}|\mathbf{u}$, which is related to the renormalized vorticity as

$$\widetilde{\mathbf{u}} = i\mathbf{o} \times \widetilde{\boldsymbol{\omega}}. \tag{6.6}$$

Using relations (6.5) and (6.6), the vorticity equation (6.1) after dropping the common factor $e^{2\tau}$ becomes

$$\partial_\tau \widetilde{\boldsymbol{\omega}} = G[\widetilde{\boldsymbol{\omega}}], \tag{6.7}$$

where the ith component of the nonlinear operator $G[\widetilde{\boldsymbol{\omega}}]$ is

$$(G[\widetilde{\boldsymbol{\omega}}])_i = -\widetilde{\omega}_i - \widetilde{u}_j * \widetilde{\partial}_j \widetilde{\omega}_i + \widetilde{\omega}_j * \widetilde{\partial}_j \widetilde{u}_i, \quad \widetilde{\partial}_j = io_j. \tag{6.8}$$

The choice of variables (6.5) is motivated by the scaling invariance: the operator $G[\widetilde{\boldsymbol{\omega}}]$ is homogeneous (invariant to translations) with respect to τ and η, which correspond to temporal and spatial scaling, respectively. In our model, the scaling invariance is represented by the shifts of η with integer multiples of $\log \lambda$. These properties allow studying the blowup as an attractor of system (6.7); see, e.g., [29, 62, 30]. For example, the self-similar blowup solution (6.4) corresponds to the traveling wave $\widetilde{\boldsymbol{\omega}} = \mathbf{W}(e^{\eta - \gamma\tau}\mathbf{o})$, which has a stationary profile in the comoving reference frame $\eta' = \eta - \gamma\tau$. In the

limit $\eta \sim \gamma\tau \to \infty$, the original variables (6.5) yield the blowup dynamics: $|\boldsymbol{\omega}| \to \infty$ and $\ell \sim 1/|\mathbf{k}| \to 0$ as $t \to t_b$. Such a blowup is robust to small perturbations if the traveling wave is an attractor in system (6.7).

Irregular evolution observed in Fig. 6.1 suggests that the attractor of system (6.7) cannot be a traveling wave. We will now argue that the attractor in the renormalized system represents a chaotic wave moving with the average speed γ. Figure 6.2 shows absolute values of the third component $\widetilde{\omega}_3$ as functions of two wave numbers $k_1 > 0$ and $k_2 > 0$ for four different values of τ; here the third wave vector component is constant and chosen at the node nearest to $k_3 = e^{\gamma\tau+6} \propto (t_b - t)^{-\gamma}$. This figure presented in log scale demonstrates a wave moving with constant speed in average $\eta \sim \gamma\tau$, but not preserving exactly the spatial vorticity distribution. In order to confirm that the wave is chaotic, we computed the largest Lyapunov exponent $\lambda_{\max} = 9.18 \pm 0.07$ in Fig. 6.3; here we added a tiny perturbation to the original solution at $\tau = 1.7$, when the attractor is already fully established, and observed the exponential deviation of the solutions $\max_{\mathbf{k}} |\delta\widetilde{\boldsymbol{\omega}}(\tau)| \propto e^{\lambda_{\max}\tau}$ in renormalized time τ. In the original variables, this yields the rapid power-law growth

$$\max_{\mathbf{k}} |\delta\boldsymbol{\omega}(t)| \propto (t_b - t)^{-\zeta}, \quad \zeta = \lambda_{\max} + 1 \approx 10.18. \tag{6.9}$$

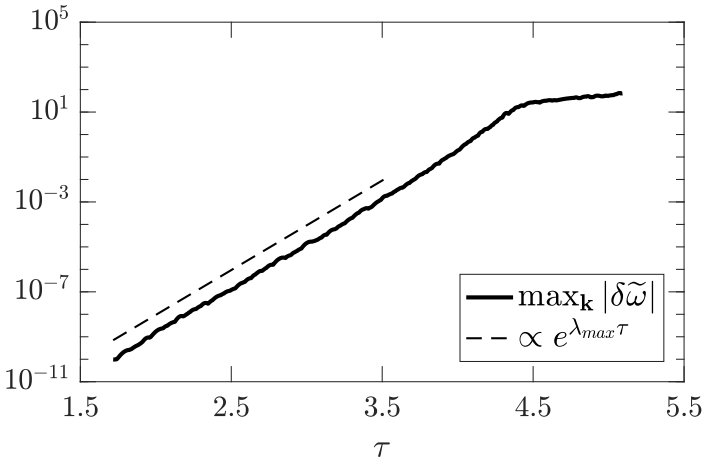

Fig. 6.3 Evolution of a small perturbation of vorticity, $\max_{\mathbf{k}} |\delta\widetilde{\boldsymbol{\omega}}|$, in renormalized variables. Solutions deviate exponentially with the Lyapunov exponent $\lambda_{\max} \approx 9.18$.

The striking property of the chaotic attractor is that it restores the isotropy in the statistical sense, even though the solution at each particular moment is essentially anisotropic, in similarity to the recovery of isotropy in the Navier-Stokes turbulence [36, 8]. This property is confirmed in Fig. 6.4 presenting the averages of renormalized

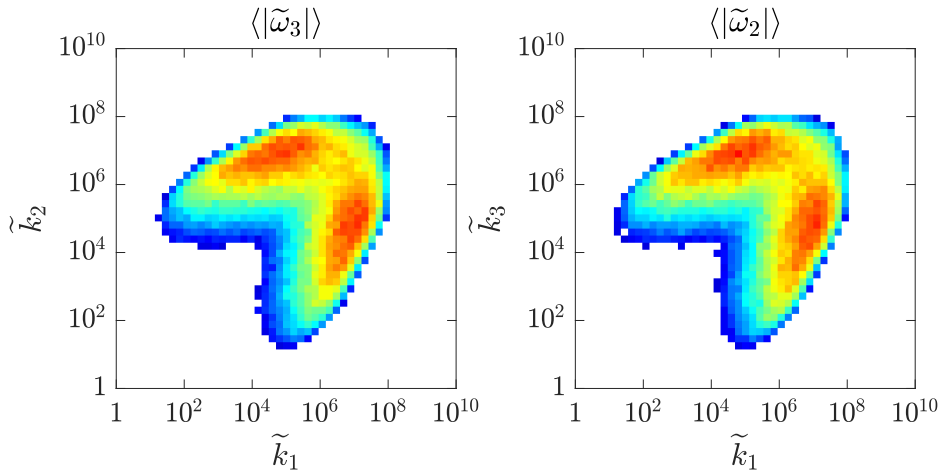

Fig. 6.4 Statistical isotropy: Left panel shows the τ average of $|\widetilde{\omega}_3|$ from Fig. 6.2 in a comoving reference frame $\eta' = \eta - \gamma\tau$. Right panel shows analogous result for the average of $|\widetilde{\omega}_2|$ on plane $(\widetilde{k}_1, \widetilde{k}_3)$. Planes of the two figures are related by the 90° rotation about the $\widetilde{k}_3$ axis. Similar results are obtained for other elements of the rotation symmetry group $\mathsf{O_h}$.

vorticity components $|\widetilde{\omega}_i|$, considered in the comoving reference frame $\eta' = \eta - \gamma\tau$. The isotropy, as well as other statistical properties, are expected to be established very rapidly in realistic conditions, e.g., in the presence of microscopic fluctuations, because of the very large Lyapunov exponent; see Eq. (6.9). This resembles closely a similar effect in developed turbulence [72].

6.3 Relation to Existing DNS

As one can infer from Figs. 6.2 and 6.4, the chaotic attractor has the span of about six decades of spatial scales. This property imposes fundamental limitations on the numerical resources necessary for the observation of blowup, assuming that the dynamics in the continuous 3D Euler equations can be qualitatively similar to our model. The approximate time limit, which would be accessible for the state-of-the-art DNS with the 8192^3 grid [41, 46, 53] can be estimated in our model as $t_{\rm DNS} \approx 9$ or $\tau_{\rm DNS} \approx -1.9$ for the renormalized time; see Fig. 6.2 (left panel). At this instant, the chaotic attractor is still at its infant formation stage and, hence, the dynamics is essentially transient. The increase of the vorticity from $\omega_{\max}(0) = 0.91$ to $\omega_{\max}(t_{\rm DNS}) = 1.89$ and of the enstrophy from $\Omega(0) = 27.2$ to $\Omega(t_{\rm DNS}) = 1.92 \times 10^3$ is moderate, which is also common for the DNS. Moreover, Fig. 6.5 shows that the growth of enstrophy and vorticity for $t \lesssim t_{\rm DNS}$ is not faster than double exponential in agreement with [47, 46, 53] – see also Fig. 1.2

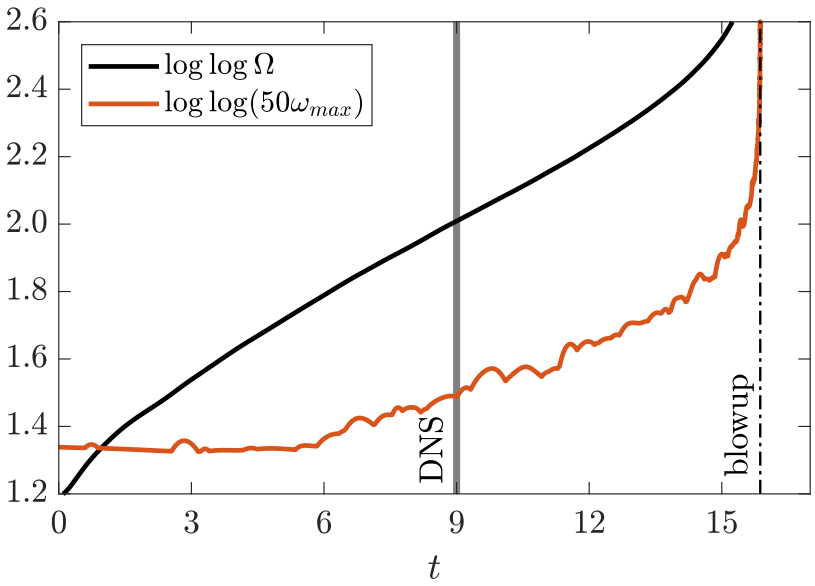

Fig. 6.5 Evolution of $\log\log\Omega$ and $\log\log(50\omega_{\max})$ for the enstrophy and maximum vorticity; the factor 50 is used to avoid complex values of the logarithm. The dash-dotted line indicates the blowup time. The vertical solid line estimates the limit $t_{\rm DNS} \approx 9$ that would be accessible for the state-of-the-art DNS with the grid 8192^3. Until $t_{\rm DNS}$, both Ω and $\omega_{\max}$ demonstrate the growth not greater than double exponential. See Fig. 1.2 for the DNS picture.

for the DNS picture. The chaotic blowup behavior offers a diversity of flow structures as it is indeed observed for different initial conditions [38]; some DNS showed the incipient development of power-law energy spectra [2], in qualitative agreement with Fig. 6.1(c).

At the time $t_{\rm DNS}$, the wave vector at the vorticity maximum is equal to $\mathbf{k}_{\max} = (\lambda^6, -\lambda^3, \lambda^{10}) \approx (18.9, -4.2, 123)$. Its third component is much larger than the other two. This has a similarity with DNS, which typically demonstrate depleting of vorticity growth within quasi-2D (thin in one and extended in the other two directions) vorticity structures [11, 37, 3]. Such dominance of one scale over the others by 1 or 2 orders of magnitude persists for larger times in our model.

Chapter 7

Conclusions

We propose a new modelling technique for the study of singularities in fluid flows. This technique considers the restriction of the Fluid Dynamics equations on logarithmic lattices in Fourier space. We classified all irreducible lattices with respect to their triad interactions and used this classification to endow the space of functions on the logarithmic lattice with an operational strucuture which mimics the usual calculus and algebraic operations between functions defined on the whole Euclidean space. This approach yields new simplified models structurally identical to the Fluid Dynamics equations and, therefore, retaining automatically many of their properties.

The capability of this technique to recover singular solutions was attested by its application to the Burgers equation. The inviscid solutions of the logarithmic model blows up in finite time, developing a power law with scaling exponent close to the known assymptotics for the continuous model, while the viscous regularized equation reproduces the discontinuous (shock) solutions in the inviscid limit $\nu \to 0$.

The application of our methodology to the Euler equations provides an intermediate approach between the full DNS and the oversimplified available toy models. It preserves not only the basic symmetries and invariants, like energy and helicity, but also a number of fine properties of the Euler flow, such as incompressibility and Kelvin's circulation theorem, in a generalized form. Moreover, it allows highly accurate numerical simulations spanning a large spatial range. Their solutions correlate with DNS in their respective scales, and still have access to a much more refined resolution.

With this technique, we propose an explanation for the existing controversy in the blowup problem for the incompressible 3D Euler equations. We show that the logarithmic model has the non-self-similar blowup, which is explained as a chaotic attractor in renormalized equations. Our results demonstrate that the blowup has enormously higher complexity than anticipated before: its "core" extends to six decades

of spatial scales. This suggests that modern DNS of the original continuous model may be unsuitable for the blowup observation.

Our approach to the blowup phenomenon is not limited to the Euler equations, but is ready-to-use for analogous studies in other fields such as natural convection, geostrophic motion, magnetohydrodynamics, and plasma physics.

References

[1] J. Aarts, R. Fokkink, and G. Kruijtzer. Morphic numbers. *Nieuw Archief voor Wiskunde*, 2:56–58, 2001.

[2] D. S. Agafontsev, E. A. Kuznetsov, and A. A. Mailybaev. Development of high vorticity structures in incompressible 3D Euler equations. *Phys. Fluids*, 27:085102, 2015.

[3] D. S. Agafontsev, E. A. Kuznetsov, and A. A. Mailybaev. Asymptotic solution for high-vorticity regions in incompressible three-dimensional Euler equations. *J. Fluid Mech.*, 813:R1, 2017.

[4] H. Andréasson. The Einstein-Vlasov system/kinetic theory. *Living Rev. Relativ.*, 14(1):4, 2011.

[5] J. T. Beale, T. Kato, and A. Majda. Remarks on the breakdown of smooth solutions for the 3-D Euler equations. *Comm. Math. Phys.*, 94(1):61–66, 1984.

[6] R. Benzi and U. Frisch. Turbulence. *Scholarpedia*, 5(3):3439, 2010.

[7] L. Biferale. Shell models of energy cascade in turbulence. *Ann. Rev. Fluid Mech.*, 35:441–468, 2003.

[8] L. Biferale and I. Procaccia. Anisotropy in turbulent flows and in turbulent transport. *Phys. Rep.*, 414(2-3):43–164, 2005.

[9] D. Biskamp. *Nonlinear Magnetohydrodynamics*. Cambridge University Press, 1997.

[10] T. Bohr, M. H. Jensen, G. Paladin, and A. Vulpiani. *Dynamical Systems Approach to Turbulence*. Cambridge University Press, 2005.

[11] M. E. Brachet, M. Meneguzzi, A. Vincent, H. Politano, and P. L. Sulem. Numerical evidence of smooth self-similar dynamics and possibility of subsequent collapse for three-dimensional ideal flows. *Phys. Fluids A*, 4:2845–2854, 1992.

[12] M. P. Brenner, S. Hormoz, and A. Pumir. Potential singularity mechanism for the Euler equations. *Phys. Rev. Fluids*, 1(8):084503, 2016.

[13] T. Buckmaster, C. De Lellis, L. Székelyhidi, and V. Vicol. Onsager's conjecture for admissible weak solutions. *Comm. Pure Appl. Math.*, 72(2):229–274, 2019.

[14] T. Buckmaster, C. De Lellis, P. Isett, and L. Székelyhidi. Anomalous dissipation for 1/5-Hölder Euler flows. *Ann. Math.*, 182(1):127–172, 2015.

[15] J.M. Burgers. A mathematical model illustrating the theory of turbulence. *Adv. in Appl. Mech.*, 1:171–199, 1948.

[16] C. S. Campolina and A. A. Mailybaev. Chaotic blowup in the 3D incompressible Euler equations on a logarithmic lattice. *Phys. Rev. Lett.*, 121:064501, 2018.

[17] D. Chae. Nonexistence of self-similar singularities for the 3D incompressible Euler equations. *Commun. Math. Phys.*, 273(1):203–215, 2007.

[18] D. Chae. Incompressible Euler Equations: the blow-up problem and related results. In *Handbook of Differential Equations: Evolutionary Equations*, volume 4, pages 1–55. Elsevier, 2008.

[19] D. Chae and R. Shvydkoy. On formation of a locally self-similar collapse in the incompressible Euler equations. *Arch. Ration. Mech. Anal.*, 209(3):999–1017, 2013.

[20] A. Cheskidov, P. Constantin, S. Friedlander, and R. Shvydkoy. Energy conservation and Onsager's conjecture for the Euler equations. *Nonlinearity*, 21(6):1233–1252, 2008.

[21] A. Cheskidov and K. Zaya. Regularizing effect of the forward energy cascade in the inviscid dyadic model. *Proc. Amer. Math. Soc.*, 144(1):73–85, 2016.

[22] Y. Choquet-Bruhat. *General Relativity and the Einstein Equations*. Oxford University Press, 2009.

[23] P. Constantin, P. D. Lax, and A. Majda. A simple one-dimensional model for the three-dimensional vorticity equation. *Comm. Pure Appl. Math.*, 38(6):715–724, 1985.

[24] P. Constantin, A. J. Majda, and E. Tabak. Formation of strong fronts in the 2-D quasigeostrophic thermal active scalar. *Nonlinearity*, 7(6):1495–1533, 1994.

[25] V. N. Desnyansky and E. A. Novikov. The evolution of turbulence spectra to the similarity regime. *Izv. Akad. Nauk SSSR, Fiz. Atmos. Okeana*, 10:127–136, 1974.

[26] P. D. Ditlevsen. *Turbulence and Shell Models*. Cambridge University Press, 2010.

[27] T. Dombre and J. L. Gilson. Intermittency, chaos and singular fluctuations in the mixed Obukhov–Novikov shell model of turbulence. *Physica D*, 111(1–4):265–287, 1998.

[28] D. G. Ebin and J. E. Marsden. Groups of diffeomorphisms and the solution of the classical Euler equations for a perfect fluid. *Bull. Amer. Math. Soc.*, 75(5):962–967, 1969.

[29] J. Eggers and M. A. Fontelos. The role of self-similarity in singularities of partial differential equations. *Nonlinearity*, 22:R1, 2009.

[30] J. Eggers and M. A. Fontelos. *Singularities: Formation, Structure, and Propagation*. Cambridge University Press, 2015.

[31] J. Eggers and S. Grossmann. Does deterministic chaos imply intermittency in fully developed turbulence? *Phys. Fluids A*, 3(8):1958–1968, 1991.

[32] T. M. Elgindi and I.-J. Jeong. Finite-time singularity formation for strong solutions to the axi-symmetric 3D Euler equations. *arXiv:1802.09936*, 2018.

[33] G. L. Eyink. Dissipative anomalies in singular Euler flows. *Physica D*, 237:1956–1968, 2008.

[34] G. L. Eyink and K. R. Sreenivasan. Onsager and the theory of hydrodynamic turbulence. *Rev. Modern Phys.*, 78(1):87–135, 2006.

[35] G. B. Folland. *Introduction to Partial Differential Equations*. Princeton University Press, 2nd edition, 1995.

[36] U. Frisch. *Turbulence: the Legacy of A.N. Kolmogorov*. Cambridge University Press, 1995.

[37] U. Frisch, T. Matsumoto, and J. Bec. Singularities of Euler flow? Not out of the blue! *J. Stat. Phys.*, 113:761–781, 2003.

[38] J. D. Gibbon. The three-dimensional Euler equations: Where do we stand? *Physica D*, 237(14-17):1894–1904, 2008.

[39] R. T. Glassey and W. A. Strauss. Singularity formation in a collisionless plasma could occur only at high velocities. *Arch. Ration. Mech. Anal.*, 92(1):59–90, 1986.

[40] E. B. Gledzer. System of hydrodynamic type admitting two quadratic integrals of motion. *Sov. Phys. Doklady*, 18:216, 1973.

[41] T. Grafke, H. Homann, J. Dreher, and R. Grauer. Numerical simulations of possible finite time singularities in the incompressible Euler equations: comparison of numerical methods. *Physica D*, 237(14):1932–1936, 2008.

[42] R. Grauer, C. Marliani, and K. Germaschewski. Adaptive mesh refinement for singular solutions of the incompressible Euler equations. *Phys. Rev. Lett.*, 80(19):4177, 1998.

[43] S. Grossmann and D. Lohse. Intermittency in the Navier–Stokes dynamics. *Z. Phys. B*, 89(1):11–19, 1992.

[44] S. Grossmann, D. Lohse, and A. Reeh. Developed turbulence: From full simulations to full mode reductions. *Phys. Rev. Lett.*, 77(27):5369, 1996.

[45] Ö. D. Gürcan. Nested polyhedra model of turbulence. *Phys. Rev. E*, 95:063102, 2017.

[46] T. Y. Hou. Blow-up or no blow-up? A unified computational and analytic approach to 3D incompressible Euler and Navier–Stokes equations. *Acta Numer.*, 18:277–346, 2009.

[47] T. Y. Hou and R. Li. Computing nearly singular solutions using pseudo-spectral methods. *J. Comp. Phys.*, 226(1):379–397, 2007.

[48] P. Isett. A proof of Onsager's conjecture. *Ann. Math.*, 188(3):871–963, 2018.

[49] Y. Kaneda, T. Ishihara, M. Yokokawa, K. Itakura, and A. Uno. Energy dissipation rate and energy spectrum in high resolution direct numerical simulations of turbulence in a periodic box. *Phys. Fluids*, 15(2):L21–L24, 2003.

[50] T. Kato. Nonstationary flows of viscous and ideal fluids in R^3. *J. Funct. Anal.*, 9(3):296–305, 1972.

[51] N. H. Katz and N. Pavlovic. Finite time blow-up for a dyadic model of the Euler equations. *Trans. Amer. Math. Soc.*, 357(2):695–708, 2005.

[52] R. M. Kerr. Evidence for a singularity of the three-dimensional, incompressible Euler equations. *Phys. Fluids A*, 5(7):1725–1746, 1993.

[53] R. M. Kerr. Bounds for Euler from vorticity moments and line divergence. *J. Fluid Mech.*, 729:R2, 2013.

[54] A. Kiselev. Small scales and singularity formation in Fluid Dynamics. In *Proc. Int. Cong. of Math.*, volume 2, pages 2329–2356, Rio de Janeiro, 2018.

[55] L. D. Landau and E. M. Lifshitz. *Quantum Mechanics: Non-Relativistic Theory*, volume 3. Butterworth-Heinemann, 1981.

[56] A. Larios, M. R. Petersen, E. S. Titi, and B. Wingate. A computational investigation of the finite-time blow-up of the 3D incompressible Euler equations based on the Voigt regularization. *Theor. Comput. Fluid Dyn.*, 32(1):23–34, 2018.

[57] J. Leray. Sur le mouvement d'un liquide visqueux emplissant l'espace. *Acta Math.*, 63:193–248, 1934.

[58] L. Lichtenstein. Über einige Existenzprobleme der Hydrodynamik homogener, unzusammendrückbarer, reibungsloser Flüssigkeiten und die Helmholtzschen Wirbelsätze. *Math. Z.*, 23:89–154, 1925.

[59] G. Luo and T. Y. Hou. Potentially singular solutions of the 3D incompressible Euler equations. *PNAS*, 111:12968–1297349, 2014.

[60] V. S. L'vov, E. Podivilov, A. Pomyalov, I. Procaccia, and D. Vandembroucq. Improved shell model of turbulence. *Phys. Rev. E*, 58(2):1811, 1998.

[61] V. S. L'vov, E. Podivilov, and I. Procaccia. Hamiltonian structure of the Sabra shell model of turbulence: Exact calculation of an anomalous scaling exponent. *EPL*, 46(5):609–612, 1999.

[62] A. A. Mailybaev. Renormalization and universality of blowup in hydrodynamic flows. *Phys. Rev. E*, 85(6):066317, 2012.

[63] A. A. Mailybaev. Continuous representation for shell models of turbulence. *Nonlinearity*, 28(7):2497–2514, 2015.

[64] A. J. Majda and A. L. Bertozzi. *Vorticity and Incompressible Flow.* Cambridge University Press, 2002.

[65] K. Ohkitani and M. Yamada. Temporal intermittency in the energy cascade process and local Lyapunov analysis in fully developed model of turbulence. *Prog. Theor. Phys.*, 89:329–341, 1989.

[66] H. Okamoto, T. Sakajo, and M. Wunsch. On a generalization of the Constantin–Lax–Majda equation. *Nonlinearity*, 21(10):2447, 2008.

[67] L. Onsager. Statistical hydrodynamics. *Il Nuovo Cimento*, 6:279–287, 1949.

[68] B. R. Pearson, P.-Å. Krogstad, and W. van de Water. Measurements of the turbulent energy dissipation rate. *Phys. Fluids*, 14(3):1288–1290, 2002.

[69] J. Pedlosky. *Geophysical Fluid Dynamics.* Springer, 2013.

[70] Private conversation with Oliver Lorscheid.

[71] A. Pumir and E. D. Siggia. Finite-time singularities in the axisymmetric three-dimension Euler equations. *Phys. Rev. Lett.*, 68(10):1511, 1992.

[72] D. Ruelle. Microscopic fluctuations and turbulence. *Phys. Lett. A*, 72(2):81–82, 1979.

[73] T. Tao. Finite time blowup for Lagrangian modifications of the three-dimensional Euler equation. *Ann. PDE*, 2:9, 2016.

[74] R. Temam. Local existence of C^∞ solutions of the Euler equations of incompressible perfect fluids. In *Turbulence and Navier Stokes Equations*, pages 184–194. Springer, 1976.

[75] C. Uhlig and J. Eggers. Singularities in cascade models of the Euler equation. *Z. Phys. B Con. Mat.*, 103(1):69–78, 1997.

[76] V. I. Yudovich. Nichtstationäre Strömung einer idealen inkompressiblen Flüssigkeit. *Zh. Vychisl. Mat. Mat. Fiz.*, 3:1032–1066, 1963.

[77] V. E. Zakharov and E. A. Kuznetsov. Hamiltonian formalism for nonlinear waves. *Phys.-Uspekhi*, 40(11):1087–1116, 1997.